FINAL REPORT

FOR

NASA GRANT NO. NSG 1295

APRIL 1, 1976 - MARCH 31, 1981

(NASA-CR-164079) STRUCTURAL RESPONSE AND INPUT IDENTIFICATION Final Report, Apr. 1976 - 31 Mar. 1981 (Lowell Univ., Mass.) 108 p HC A06/MF A01 CSCL 20K

N81-20465

Unclas
G3/39 41894

STRUCTURAL RESPONSE

AND

INPUT IDENTIFICATION

SUBMITTED BY

G. DUDLEY SHEPARD
JOHN C. O'CALLAHAN
JOHN A. MCELMAN

MARCH 27, 1981

UNIVERSITY OF LOWELL
LOWELL, MASSACHUSETTS 01854

FOREWORD

This is the final report on work performed under NASA Grant No. NSG 1295. The grant is entitled "Dynamic Response and Input Identification". The work was performed at the University of Lowell, Lowell, Massachusetts. Research investigators were Dr. John A. McElman, Dr. John C. O'Callahan and Dr. G. Dudley Shepard. Graduate research assistants assigned to this grant were Christopher Gianaeopoulos, John R. Crischow and Chaur-Ming Chow. Dr. Robert W. Fralich was the grant monitor assigned by the NASA during the first phase of this study. This work is described under Part I of this report. Dr. Michael Card was the grant monitor assigned by the NASA during the second phase of this study. This work is described under Part II of this report.

TABLE OF CONTENTS

TABLE OF CONTENTS (cont'd)

1.0 Preface

The research supported by NASA Grant NSG1295 had at the outset three major goals:

1. To develop a general method for determining the response of a structure to combined base and acoustic random excitation.
2. To develop parametric relationships to aid in the design of plates which are subjected to random force or random base excitation.
3. To develop a method to identify the individual acoustic and base inputs to a structure with only a limited number of measurement channels, when both types of excitation act simultaneously.

A discrete method of analysis was chosen early in this study because it provided the flexibility necessary to analyze any type of structure that might be encountered. Study of both the response and the input identification problems led to the development of a computer program which requires as input only the modal parameters of the structure (natural frequencies, mode shapes, and damping ratios) and appropriate excitation or response spectra. This approach is ideally suited to be coupled with a finite element program.

This study included both analytical and experimental work, and it is useful to emphasize the inherent contrast between these two approaches. In the theory-based analytical phase of this study, questions were first posed and then answered by the analyst,

whereas in the experimental phase, the questions were posed by the experimental data itself. The experimenter was then challenged to find answers to questions which were often unanticipated. The reporting of this study has fallen naturally into two parts, one which describes the theory based approach and the other which describes the experimental reality.

2.0 Symbol List

English

a	Fourier transformed input acceleration vector
A	cross section area of acoustic transmission line
c	speed of sound in air
C	damping matrix
C_{fa}	coincident component of force and base acceleration cross power spectrum
D	spatial distribution matrix
E	elastic modulus
f	force vector
g	acceleration of gravity
G	power spectral density (PSD)
H	transfer function matrix
I	identity matrix
L	length of acoustic transmission line
m	mass; also modal degree of freedom index
M	mass matrix
n	physical degree of freedom index
$N(\omega)$	Fourier spectrum of noise source
p	pressure; also transfer function pole
P(s)	characteristic function for transfer function poles
q	modal displacement vector
Q	generalized force; also quality factor of resonance
Q_{fa}	quadrature component of force and base acceleration cross power spectrum
S	Laplace transform variable
t	time; also plate thickness

Greek

β	frequency ratio ω/ω_n; also plate aspect ratio
γ^2	coherence ratio
Γ	modal participation factor
$\Delta(s)$	characteristic function
ζ	damping ratio
η	material damping loss factor
ν	Poisson's ratio
$\xi(x,t)$	displacement function
ρ	mass density
ψ	cross spectrum phase angle
ω	frequency, radians/sec.
ω_n	natural frequency

Subscripts

a	base acceleration input process
f	force input process
M	material
p	plate
r	response variable
s	specific; also shaker
y	plate deflection response process

Superscripts

*	complex conjugate
·	time differentiation
$(\bar{})$	(overbar) implies a modal vector or matrix

English (continued)

U	modal transformation matrix
$W(\omega)$	Fourier spectrum of output signal
x	axial coordinate for acoustic transmission line
$X(\omega)$	Fourier spectrum of input signal
y	plate deflection response vector
Y	Fourier spectrum of response signal
z	transfer function zero
Z(s)	characteristic function for transfer function zeros

3.0 List of Figures and Tables

4.0 Part I: Theory-Based Models for Structural Response and Input Identification

4.1 Introduction to Part I

The estimation of the vibration response of a continuous structure to a spatially distributed wide-band random excitation combines essentially two problems: the identification of the dynamic properties of the structure and the handling of the statistics of the multiple excitation and response variables. The inherent computational complexity of dealing with many variables which are both dynamically and statistically coupled often means that for real engineering structures the level of detail is limited by cost.

At present solutions to the response problem use either the classic transfer function approach or the non-classical method of statistical energy analysis (SEA).[1] Broadly speaking, classical methods which use continuous system models[2] offer excellent spatial and frequency resolution but are limited to highly idealized structures with simplified boundary conditions. Classical methods based on finite system models can handle more realistic engineering structures but the cost limit on the number of degrees of freedom in turn limits spatial resolution and frequency bandwidth. Finally, the SEA method offers wide-band frequency estimates at the expense of reduced spatial detail caused by the crude averaging of the spatial modes of response.

This study uses the classical approach on a finite system model. It is assumed that the system is known in terms of its natural modes and frequencies from either existing analytical solutions or

from a finite element program. Damping ratio assumptions are made separately based on experimental data. An efficient computational strategy called Program RAND is then developed to perform both dynamic response and input identification calculations for a multi-degree-of-freedom (MDOF) structure subjected to statistically coupled pressure and base excitation.

4.2 Development of Program RAND

4.2.1 Analysis

The analysis proceeds in two steps. First, it is necessary to perform a signal analysis, i.e., to trace the effect of the input vector through the structure to the resulting output response vector. Next, a statistical analysis is made to determine the space and time correlations between the input and output vectors.

Consider first the case of a continuous structure excited by a force process which is randomly distributed in space and time. The structure is divided into n discrete elements. An n-dimensional force vector f(t) causes a displacement response described by an n-dimensional displacement vector y(t). In the usual fashion the modal transformation

$$y = Uq \tag{4-1}$$

is used to transform the original governing matrix differential equation into the decoupled modal equation

$$\bar{M}\ddot{q} + \bar{C}\dot{q} + \bar{K}q = Q \tag{4-2}$$

where U is the undamped modal matrix, $\bar{M}$, $\bar{C}$, $\bar{K}$ are diagonal modal property matrices, and the modal force vector $Q = U^T f$. Such a transformation exists whenever C is proportional to K or M; the

transformation is approximately valid for non-proportional damping whenever the damping is light.

For reasons of economy of computation it is desirable to deal with a reduced number of modal equations and modal coordinates equal to m, where $m < n$. Such a reduction is warranted, for instance, whenever a mode does not significantly contribute energy to the overall response. So the matrices $\bar{M}$, $\bar{C}$, and $\bar{K}$ are of order (m x m), and U is of order (n x m).

Since each mode is governed by a scalar equivalent to the matrix equation (4-2), a modal transfer function can be obtained by Fourier transformation for each modal coordinate. For instance, for the p^{th} mode

$$q_p = Q_{s,p} H_p(\omega) \tag{4-3}$$

where $Q_{s,p} = Q_p/M_p$ is the specific modal force. When all the mode response amplitudes are known the modal response vector q must be transformed back to the physical space vector y by the transformation (4-1).

All of the preceding signal operations that are required to relate the vectors f and y can be summarized in the signal vector block diagram shown in Figure 4-1.

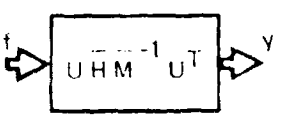

Fig. 4-1 Force Input Transfer Matrix

This diagram uses the convention that the output vector is obtained by premultiplying the input vector by the transfer matrix. The matrix $\bar{H}(\omega)$ is a diagonal modal transfer function matrix consisting of the individual transfer functions $H_p(\omega)$. The physical-space transfer matrix H_f is seen to be related to the modal-space transfer matrix by the equation

$$H_f = U \bar{H} \bar{M}^{-1} U^T \tag{4-4}$$

Next the statistical relations which correspond to the signal vector block diagram can be determined by Fourier transforming related time domain correlation matrices. For instance, to the real coordinate transformation $y = Uq$ there corresponds the frequency domain power spectrum relation

$$G_y(\omega) = U G_q(\omega) U^T \tag{4-5}$$

and where the elements of G refer to the one-sided spectra customarily used in engineering calculations, and the single subscripts y and q refer to the y and q vector processes, respectively. This simple notation has been used rather than the more customary double subscript notation in order to avoid confusion later when more than one input vector process contribute to the overall response. For the complex transformation $q = H(\omega)\, Q_s$ the statistical relation is

$$G_q(\omega) = H^*(\omega)\, G_{Q_s}(\omega)\, H^T(\omega) \tag{4-6}$$

where the (*) denotes the complex conjugate. All the other transformations implied by the matrix products in equation (4-4) are real, and they will each have a power spectrum relation similar to equation (4-5). The overall power spectrum relation between the

input vector process f and the output process vector y is then

$$G_y = U\, H^* \bar{M}^{-1}\, U^T G_f U\, \bar{M}^{-1}\, H\, U^T \qquad (4\text{-}7)$$

where the indication of the dependence on the frequency ω has been dropped and the substitutions $M^{-T} = M^{-1}$ and $H^T = H$ have been made. From an operational point of view the response spectrum matrix in equation (4-7) is obtained in the same manner as in equation (4-6): that is, by premultiplying the input spectrum matrix by the conjugate transfer matrix H_f^* and post-multiplying by the transposed transfer matrix H_f^T.

The above procedure of first developing the vector signal block diagram and then drawing out the corresponding power relations provides a powerful and convenient operational tool for more complicated processes. As a second example, consider the response of a continuous structure to a base input which is uniform spatially but random in time. The vector signal relation between a, the Fourier transform of the base input acceleration vector x(t), and the Fourier transformed absolute displacement response vector y has the block diagram representation shown in Figure 4-2. Taken as a whole, the transformations in Figure 4-2 constitute

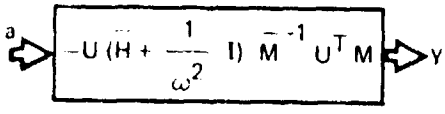

Fig. 4-2 Base Input Transfer Matrix

the physical-space transfer matrix

$$H_a = U(\bar{H} + \frac{1}{\omega^2} I)\, \bar{M}^{-1}\, U^T M \qquad (4\text{-}8)$$

To draw out the power relations for this process the same operational approach used in the previous example is followed:

$$G_y = U(\bar{H}^* + \frac{1}{\omega^2} I)\, \bar{M}^{-1}\, U^T M\, G_a\, M\, U\, \bar{M}^{-1} (\bar{H} + \frac{1}{\omega^2} I) U^T \qquad (4\text{-}9)$$

where again matrix transposition has been omitted for the symmetric matrices M, $\bar{M}^{-1}$, $\bar{H}$.

As a third example, the previous two examples are combined by assuming that the force excitation and base excitation processes act simultaneously on the structure, and further, that they are statistically coupled. The vector signal block diagram for this case is shown in Figure 4-3.

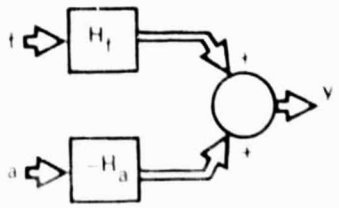

Fig. 4-3 Combined Input Vector Processes

To draw out the power relations for the process shown in Figure 4-3 the same operational approach is followed as with the previous examples. There is, however, a new block diagram operation of summing statistically coupled vectors which requires a

corresponding new power relation. This relation can be written in the following partitioned matrix form:

$$G_y = \begin{Bmatrix} H_f^* \\ \hline -H_a^* \end{Bmatrix}^T \left[\begin{array}{c|c} G_f & G_{fa} \\ \hline G_{af} & G_a \end{array}\right] \begin{Bmatrix} H_f^T \\ \hline -H_a^T \end{Bmatrix} \qquad (4\text{-}10)$$

where G_{fa} is the cross power spectral density matrix which describes the statistical coupling between the f and a input processes. The compact relation of equation (4-10) is more easily interpreted in the expanded form:

$$G_y = H_f^* G_f H_f^T - H_f^* G_{fa} H_a^T - H_a^* G_{af} H_f^T + H_a^* G_a H_a^T \qquad (4\text{-}11)$$

The first term on the right-hand side of equation (4-11) is given by equation (4-7); the last term is given by equation (4-9). Each of the middle two terms, because they represent cross power terms between two separate vector processes, are non-symmetric matrices. They are, however, conjugate transposes of each other, so that their sum yields a matrix with the Hermitian symmetry required for G_y.

As a final example, consider the input identification problem associated with the system shown in Figure 4-3. It is assumed that the output process and only one of the two statistically coupled input processes are known. For example, imagine that the signal vectors $y(t)$ and $f(t)$ are known and are available for statistical processing but that the spectral matrices G_a and G_{fa} associated with the base input process are not known. If the cross process

matrix G_{fa} were known, it would in principle be possible to rearrange equation (4-11) and to reconstruct the unknown matrix G_a. As an alternative, since y(t) and f(t) are available, it is possible to compute another cross power matrix G_{fy}. The additional information provided by G_{fy} makes possible the deduction of both G_a and G_{fa}. We consider here only the reconstruction of G_a. The strategy for this approach is based on the following partitioned cross power relation for the system shown in Figure 4-3:

$$\left\{\begin{array}{c} G_{fy} \\ \hdashline G_{ay} \end{array}\right\} = \left[\begin{array}{c:c} G_f & G_{fa} \\ \hdashline G_{af} & G_a \end{array}\right] \left\{\begin{array}{c} H_f^T \\ \hdashline -H_a^T \end{array}\right\} \tag{4-12}$$

The upper matrix equation of equation (4-12) is

$$G_{fy} = G_f H_f^T - G_{fa} H_a^T \tag{4-13}$$

Premultiply equation (4-13) by H_f^* and substitute into equation (4-11) to obtain

$$H_a^* G_a H_a^T = G_y + H_f^* G_f H_f^T - (H_f^* G_{fy} + G_{yf} H_f^T) \tag{4-14}$$

This equation can be used to determine G_a in terms of spectrum matrices derivable from the input processes f(t) and the output process y(t).

In a similar fashion an equation for $H_f^* S_f H_f^T$ can be obtained:

$$H_f^* G_f H_f^T = G_y + H_a^* G_a H_a^T + (H_a^* G_{ay} + G_{ya} H_a^T) \tag{4-15}$$

This equation can be used to determine G_f in terms of spectrum matrices derivable from the input process x and the output process y.

Response estimation by the use of equation (4-11) and input identification by the use of equations (4-14) and (4-15) appears deceptively simple. In fact, the amount of computation and measurement effort implied by these equations can be quite large. The questions of computational strategy and efficiency are taken up in the next section.

4.2.2 Computational Strategies and Efficiency:

Program RAND is designed to efficiently compute power spectral density (PSD) and integrated power spectral density (IPSD) for two modes of operation: a forward (i.e., response) analysis and a backward (i.e., input identification) analysis. A basic program strategy is that the major portion of the computations are performed in a reduced modal space. The modal space is determined by examining the modal power participation matrices (described below) and selecting only those modes which actively generate significant response power. In general, the number of active modes m is less than the number of original physical degrees of freedom n, and the original system equations are reduced to a smaller and simpler uncoupled set.

Further program efficiency is obtained by segregating the real and imaginary parts of complex matrices in such a way that complex matrix multiplication is replaced by a real dyadic operation called an overlay multiplication. Another program efficiency is provided which allows the user to spatially window a specific node in the system and to determine the power spectrum or integrated power spectrum for that node alone in all forward or backward modes of operation, thereby reducing computation as well as printout.

4.2.3 Method of Response Computation:

Equation (4-11) can be recast into a compact notation as

$$G_r = G_{r/f} + G_{r/a} - G_{r/fa} \tag{4-16}$$

where the "r" subscript implies the response variable which can be displacement (y), velocity ($\dot{y}$), and acceleration ($\ddot{y}$). The "/" symbol denotes "the response with respect to"; f implies force input, a the acceleration input, and fa, the cross power between the force and base inputs. Therefore, $G_{r/f}$ is the partial response PSD due to a force input only; $G_{r/a}$ is the partial response PSD for base acceleration only, and $G_{r/fa}$ is the partial response due to the cross PSD between the two random input processes. G_r is the total response power and could be written as

$$G_r = G_{r/f,\ a,\ fa} \tag{4-17}$$

As indicated earlier, the majority of the operations are performed in modal space. The transformation from modal space to the physical domain is performed by the operation

$$G_r = U\bar{G}_r U^T \tag{4-18}$$

where the bar over the response PSD denotes a modal quantity. Therefore, equation (4-16) can be reformed into a modal expression as

$$\bar{G}_r = \bar{G}_{r/f} + \bar{G}_{r/a} - \bar{G}_{r/fa} \tag{4-19}$$

The input power spectra are assumed to be separable in time and space; therefore, the partial power spectra become

$$G = G(\omega)\ D \tag{4-20}$$

where D is a matrix which describes the spatial correlation between the response degrees of freedom or the two random input processes. The modal partial PSD in equation (4-19) can be written as

$$\bar{G}_{r/f} = G_f(\omega)\ \bar{H}_f^{*}\ \bar{D}_f\ \bar{H}_f^{T} \tag{4-21}$$

$$\bar{G}_{r/a} = G_a(\omega)\ \bar{H}_a^{*}\ \bar{D}_a\ \bar{H}_a^{T} \tag{4-22}$$

$$\bar{G}_{r/fa} = (C_{fa}(\omega) + jQ_{fa}(\omega))\ (\bar{H}^{*}(\bar{D}_{fa} + \bar{D}_{fa}^{T})\ \bar{H}^{T}) \tag{4-23}$$

where C_{fa} and Q_{fa} are the coincident and quadrature components of the cross PSD of the force and base inputs, $\bar{H}_f = \bar{H}$ is the modal transfer function relating modal force to displacement, and $\bar{H}_a = \bar{H} + (1/\omega^2)\ I$ is the base acceleration modal transfer function.

The $\bar{D}$ matrices are modal power participation matrices which are used in the response analysis to identify modes which actively generate significant power. The modal distribution matrices can be expressed as

$$\bar{D}_f = \bar{M}^{-1}\ U^{T}\ D_f\ U\ \bar{M}^{-1} \tag{4-24}$$

$$\bar{D}_a = \bar{M}^{-1}\ U^{T}\ M\ D_a\ M\ U\ \bar{M}^{-1} \tag{4-25}$$

$$\bar{D}_{fa} = \bar{M}^{-1}\ U\ D_{fa}\ M\ U\ \bar{M}^{-1} \tag{4-26}$$

where the unbarred D's represent the spatial distribution matrices in the physical domain. Note that the modal power participation matrices need only be computed once and that they remain constant throughout the problem solution. Also, the complex operations in the above equations are performed using the special overlay multiplications.

The complete output information for every degree of freedom is not always needed. In that case the response matrix can be spatially windowed at a selected node i. This process will produce only the real co-power term since the quad-power term for a main diagonal element is always zero. A row matrix can be formed by partitioning the i^{th} row from the modal matrix and designating it as p_i^T. The scalar power at node i then becomes

$$G_r^i = p_i^T G_r p_i \tag{4-27}$$

where the superscript i indicates that a windowing process has been imposed on the physical PSD matrix.

The integrated PSD is obtained by an Euler integration process applied to matrices in modal space. This scheme was selected since it only requires the PSD matrices at step ω_k, thereby avoiding the difficulties of saving previously evaluated matrices for integration. Therefore, the integrated PSD is

$$\hat{G}(\omega_k) = G(\omega_{k-1}) + \frac{G(\omega_k)}{2} [\Delta\omega_k + \Delta\omega_{k-1}] \tag{4-28}$$

where ($\hat{}$) symbol denotes a modal integrated PSD and where $\Delta\omega_k = \omega_{k+1} - \omega_k$ is the new step, and $\Delta\omega_{k-1} = \omega_k - \omega_{k-1}$ is the old step.

The rate at which the program steps through frequency solution is determined automatically by the program which uses the half power width of the nearest mode as its basic step in

frequency. In order to ensure convergence or to improve accuracy, the program allows for subdividing steps and/or concentrating computations at selected modes of importance.

4.2.4 Method of Input Identification Computations:

The general problem of identifying a spatially non-uniform input process is very complex both computationally and experimentally. A reasonable level of complexity can be obtained by assuming both force and base acceleration input distributions are spatially uniform. Therefore, D_f and D_a are set to a one matrix and the input identification process is performed at a single nodal point on the structure which would correspond to an experimental accelerometer output.

To estimate the base acceleration input PSD, equation (4-14) can be written as

$$G_{r/a} = G_{r/f,a,fa} + G_{r/f} - G_{fr/f,a,fa} \qquad (4\text{-}29)$$

where $G_{r/a}$ is the partial power response due to the input base acceleration, to be identified,

$G_{r/f,a,fa}$ is the total response of the system due to all effects,

$G_{r/f}$ is the partial response due to the uniform force input PSD,

$G_{fr/f,a,fa}$ is the cross power between the input force PSD and the response of the system due all effects.

As discussed previously, it is not reasonable to require an experiment to produce all the data required to specify equation (4-29)

completely. Therefore, the windowing process must be applied to reduce equation (4-29) to

$$G^i_{r/a} = G^i_r + G^i_{r/f} - G^i_{fr} \qquad (4\text{-}30)$$

Note that the subscripts to the first and third terms have been dropped since they are the responses due to all effects. Equation (4-30) implies the following:

G^i_r is the accelerometer response at nodal position i

$G^i_{r/f}$ is the input force PSD at nodal position i which by assumption is the same at any node

G^i_{fr} is the cross PSD information between the input force PSD and the output accelerometer at node i. This PSD contains a coincident and quadrature component.

To determine an estimate of the input base acceleration PSD, the program applies a white noise PSD to the base in order to characterize the system power response, denoted as $G_{r/a'}$. Then the base input to node i can be written as

$$G^i_{r/a} = G^i_a(\omega)\, G^i_{r/a'} \qquad (4\text{-}31)$$

where $G^i_a(\omega)$ is the identified base input acceleration PSD obtained from information at node i. Solving for G^i_a using equations (4-30) and (4-31) produces

$$G^i_a(\omega) = \frac{1}{G^i_{r/a'}} [G^i_r + G^i_{r/f} - G^i_{fr}] \qquad (4\text{-}32)$$

In a similar fashion, equation (4-15) can be windowed at node i as

$$G^i_{r/f} = G^i_r + G^i_{r/a} + G^i_{ar} \qquad (4\text{-}33)$$

where G^i_{ar} is the cross PSD between the base acceleration and accelerometer output as node i. As in the previous case, a white noise force PSD is applied to obtain the force power response $G_{r/f'}$. Then the identified force input PSD obtained from information at node i is

$$G^i_f(\omega) = \frac{1}{G^i_{r/f'}} [G^i_r + G^i_{r/a} + G^i_{ar}] \qquad (4\text{-}34)$$

4.3 Results of RAND Computations

4.3.1 Combined Base and Acoustic Excitation of a Simple Oscillator:

The combined base and acoustic excitation of a simple oscillator has been studied both analytically and by using Program RAND. Originally the exact analytical solution for this case was developed to rigorously check the program logic of RAND. However, since the simple oscillator is a prototype for each of the modes of a MDOF system, the analytical solution gives valuable insight into the convergence and resolution properties of the discrete frequency operations of RAND.

For example, consider the acceleration response of a one DOF system of mass m, natural frequency ω_n, and damping ratio ζ. For the combined force and base excitations characterized by the spectra $G_f(\omega)$, $G_a(\omega)$, and $C_{fa}(\omega) + jQ_{fa}(\omega)$ the response is

$$G_{\ddot{y}}(\omega) = \frac{1}{(1-\beta^2)^2 + (2\zeta\beta)^2} \times \left[\beta^4 \frac{G_f}{M^2} - 2\beta^2 \left(\frac{C_{fa}}{M} - 2\zeta\beta \frac{Q_{fa}}{M}\right) + (1 + 4\zeta^2\beta^2)\, G_a(\omega)\right] \qquad (4\text{-}35)$$

where $\beta = \omega/\omega_n$. The term which contains C_{fa}, the coincident component of the cross power, appears with a negative sign. This reflects the fact that the separate responses to the force and to the base inputs are in opposition to each other. In contrast, the term which contains Q_{fa}, the quadrature component of the cross power, appears with a positive sign and has a smaller magnitude than the C_{fa} term, at least for $2\zeta\beta < 1$. For the case where the input spectra are constant with frequency the integrated mean squared acceleration response is

$$\langle \ddot{y}^2 \rangle = \lim_{\beta\to\infty} \left\{ \frac{G_f \omega_n}{m^2} \left[\beta + \frac{\pi(1 - 4\zeta^2)}{4\zeta} \right] - \frac{2C_{fa}\omega_n}{m} \frac{\pi}{4\zeta} + \frac{2\zeta Q_{fa}\omega_n}{m} \left[\ell n(1-2(1-2\zeta^2)\beta+\beta^2) - 1 + \frac{\pi(1-2\zeta^2)}{2\zeta\sqrt{1-\zeta^2}} \right] + G_a\omega_n \frac{\pi(1+4\zeta^2)}{4\zeta} \right\} \qquad (4\text{-}36)$$

The terms involving π represent the overall output power contributed by the resonant portion of the transfer functions. Additional terms involving β are non-resonant contributions to the output which continue to grow with frequency. Since the resonant contributions occur just in the narrow band of frequency at ω_n, a good estimate of the integrated response over a finite bandwidth which includes the resonance can be obtained by dropping the limiting operation $\beta\to\infty$ in equation (4-36).

An idea of the extreme range of the input coupling effect can be obtained by examining the special case where $Q_{fa} = 0$ and $G_a = G_f/m^2 = C_{fa}/m = G_0$. This corresponds to the case where the force and base inputs are fully coherent and the resonant contri-

butions of the two input spectra are nearly equal. Substitution into equation (4-36) yields, for the finite upper frequency ratio β,

$$\langle \ddot{y}^2 \rangle \approx G_0 \omega_n \beta \tag{4-37}$$

Thus the resonant contributions cancel each other and only the non-resonant response remains. By changing the phase of the co-power term, $C_{fa}/m = -G_0$, the overall response becomes

$$\langle \ddot{y}^2 \rangle \approx G_0 \omega_n \left(\beta + \frac{\pi}{\zeta}\right) \tag{4-38}$$

where the power contribution due to resonance is four times that caused by G_f or G_a alone. Figure 4-4 shows the results of a RAND computation for a related extreme case where $Q_{fa} \neq 0$. The phase between the base and force input is described by the phase angle $\psi = \tan^{-1} (Q_{fa}/C_{fa})$.

In summary, the resonant power response ranges from near zero (coherent signals cancel), up through a factor of two (simple sum of uncorrelated powers) to a maximum of four (coherent signals add for a signal factor of two, a power factor of four). Note that this range will be reduced whenever the inputs are not equal or are not fully coherent. It is clear that the effect of coherence and phase of the cross power can be very significant. Similar effects are apparent in MDOF system responses, to be discussed later.

4.3.2 Acoustic Excitation of a Beam

A simple ten degree-of-freedom beam was chosen to investigate the effects of the spatial correlation of the acoustic input and the effects of the beam boundary conditions. Figure 4-5 shows the center node acceleration response PSD when the beam is clamped

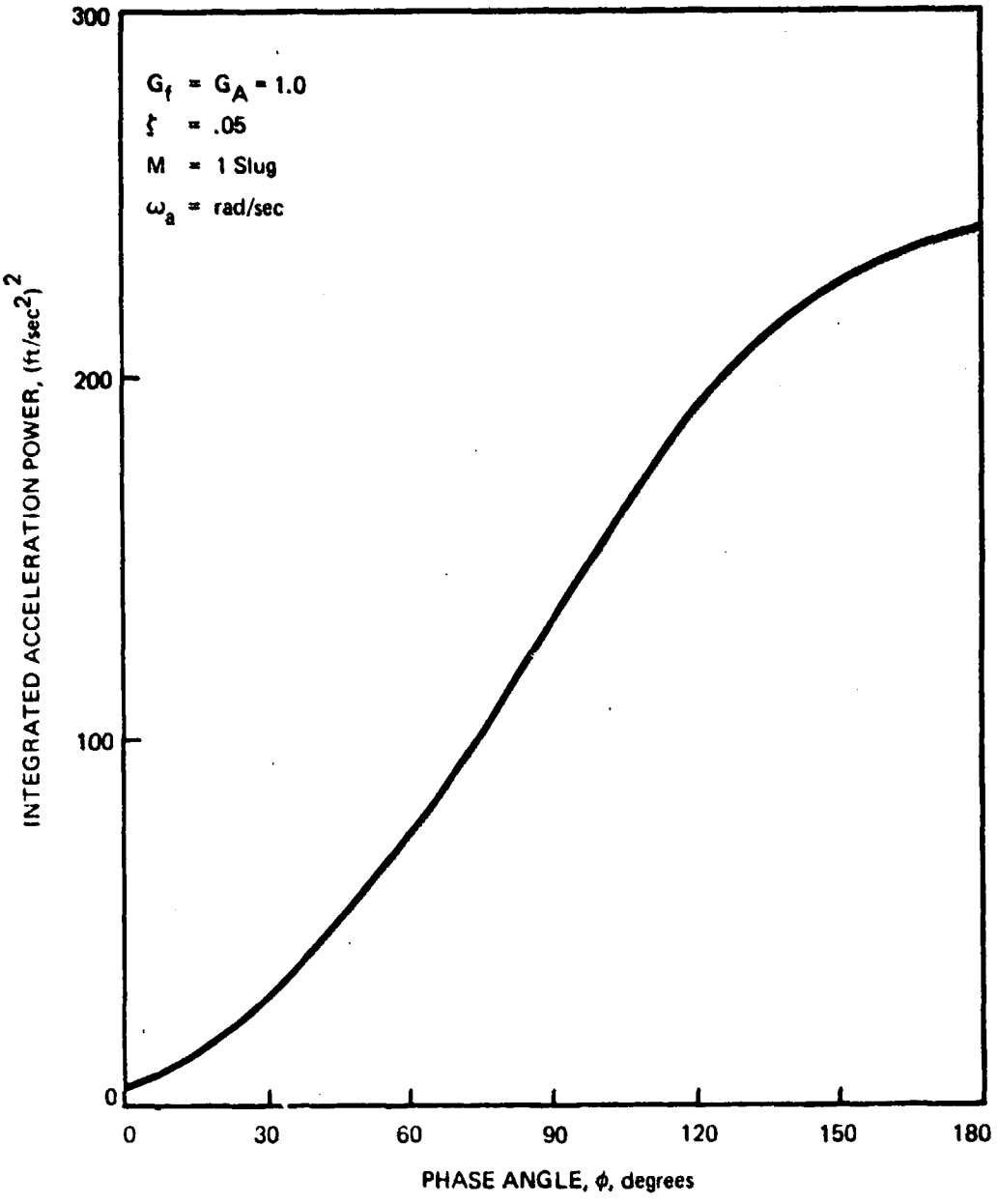

Fig. 4-4 Extreme Response Power vs Input Phase for Simple Oscillator

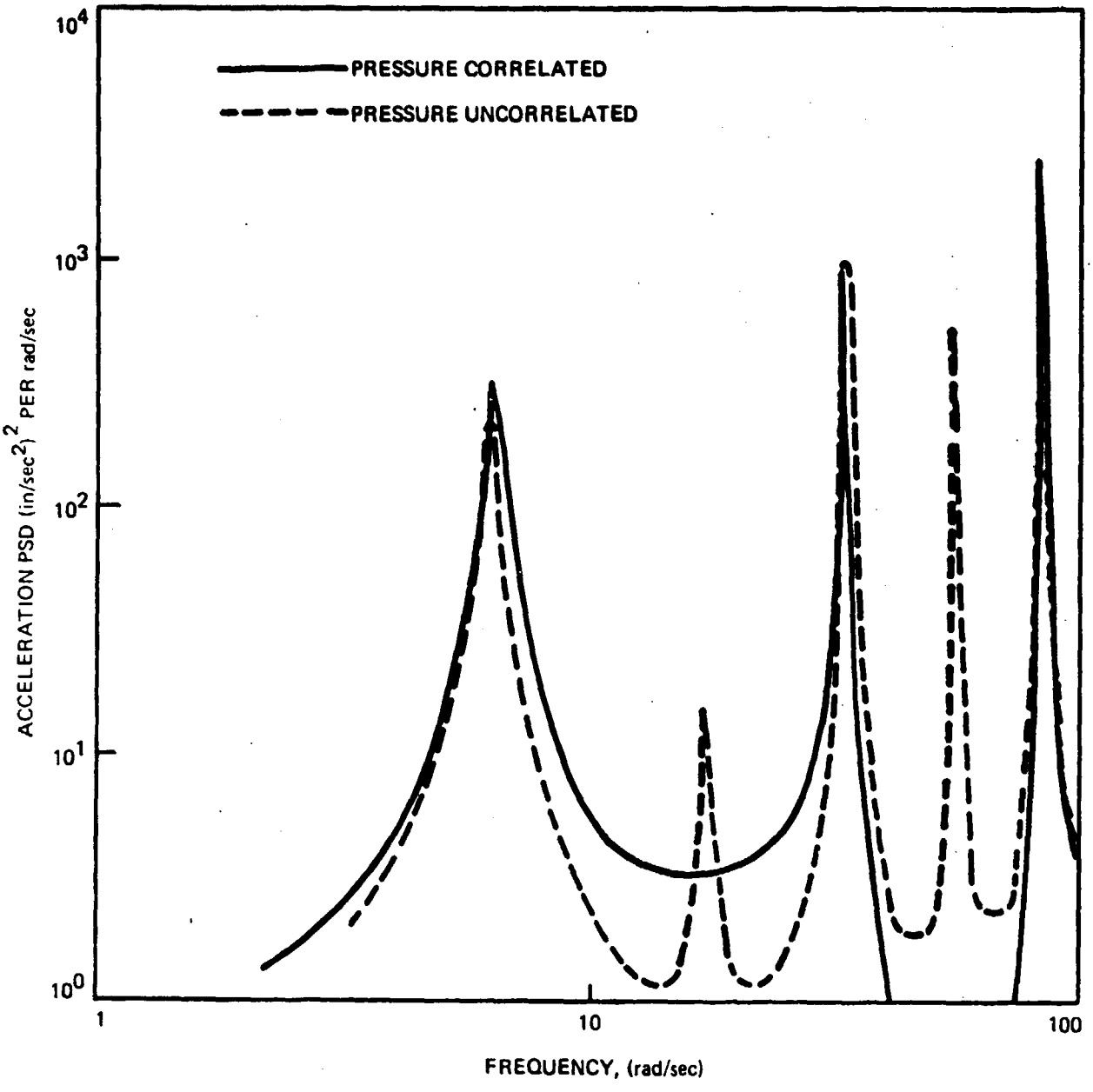

Fig. 4-5 Effect of Pressure Correlation on Beam Response PSD

at each end and is subjected to a base input as well as either a spatially correlated pressure input (solid line), or a spatially uncorrelated pressure input (dashed line). All inputs are constant with frequency (white noise) and no correlation exists between the base or acoustic inputs. It is evident that the asymetric modes (every other mode) do not participate in the response when the pressure is spatially correlated. Participation is strong for these modes, however, when the pressure is spatially uncorrelated. The area under the uncorrelated curve is, therefore, larger than that under the uncorrelated curve, resulting in a higher integrated response for the uncorrelated case.

Figure 4-6 shows the effect of boundary conditions on the integrated acceleration power response. The solid line represents simple supports while the dashed line represents clamped supports. The discrete jumps in the curves occur every time that a participating mode is passed. Since the simply supported beam has the lowest natural frequency, its response starts to build first. The two curves then alternate in height for a time until the clamped curve finally begins to maintain a higher integrated value than the simply supported curve. These results indicate that stiffer boundary conditions will give a somewhat higher integrated response, but it is felt that this will not be a major variable in response or input prediction.

Figure 4-7 shows a family of backbone curves for integrated response of the beam center node versus phase angle $\psi = \tan^{-1}(Co/Qd)$ of the cross power between the base and spatially uniform acoustic

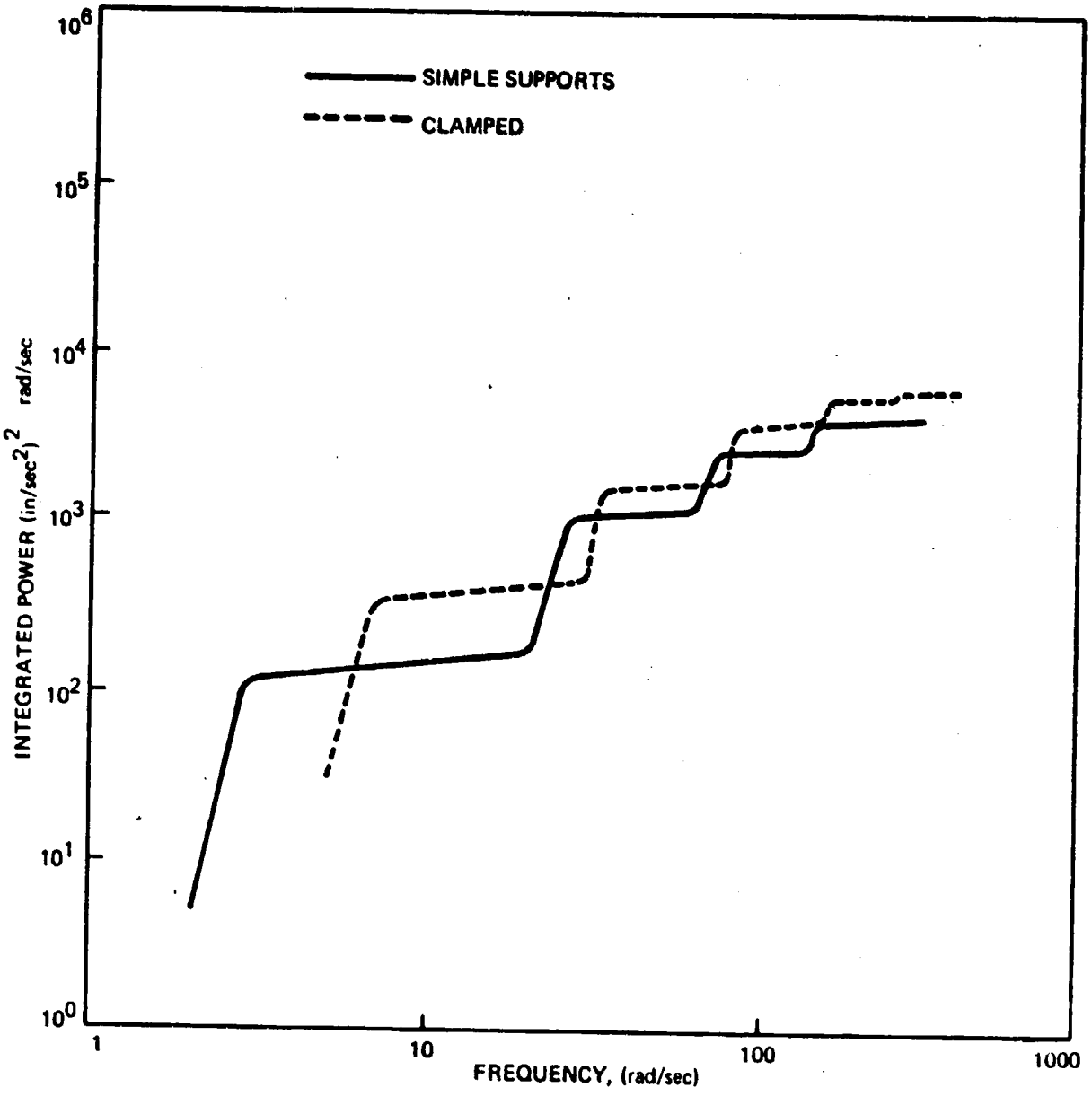

Fig. 4-6 Effect of Boundary Conditions on Integrated Response Power of Beam

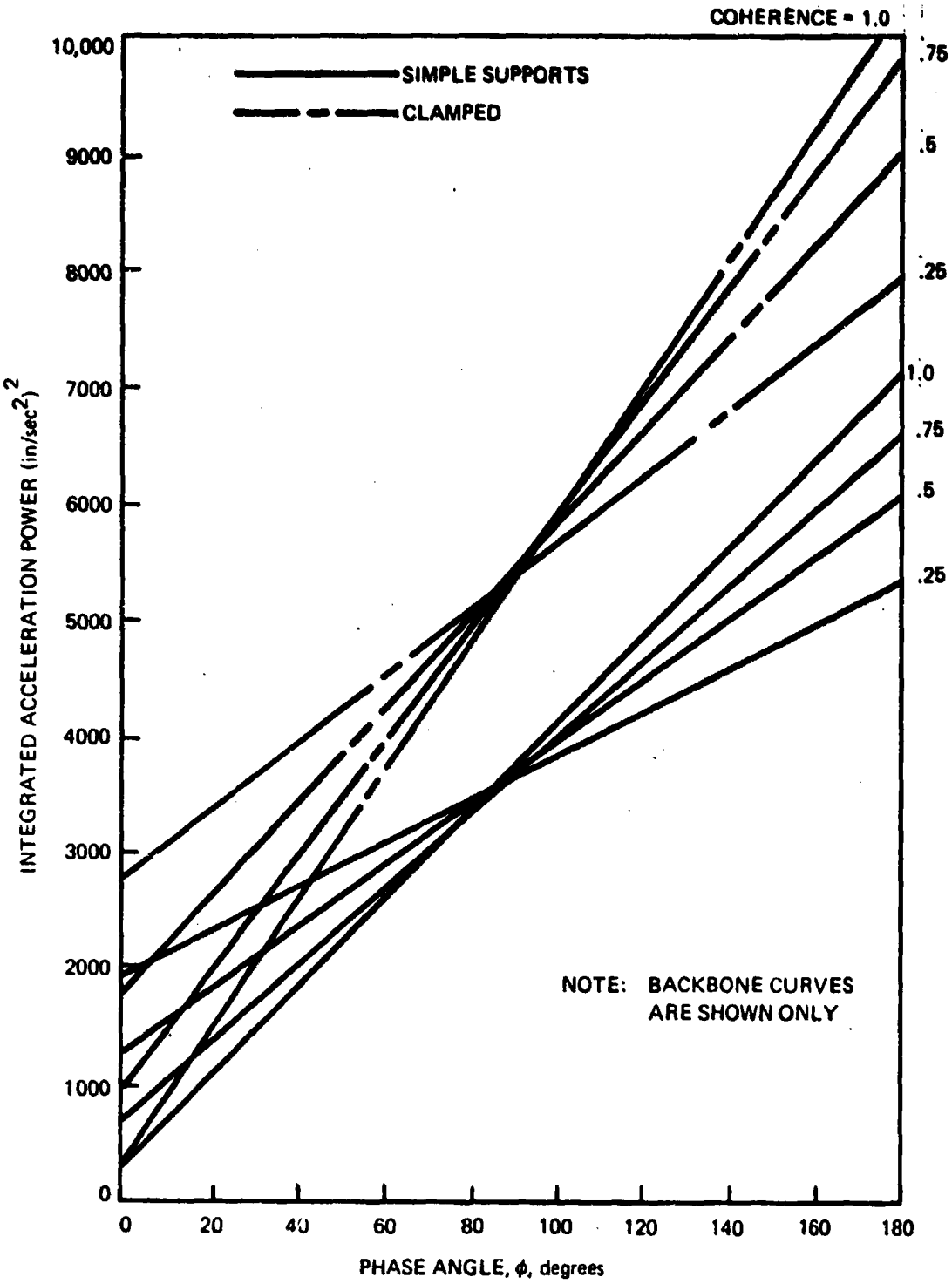

Fig. 4-7 Integrated Response Power of Beam vs. Cross PSD Phase and Coherence

inputs, for two support conditions. Omitted is the cosine-like variation with respect to each straight backbone line. (Each of actual curves in the family would have shapes similar to the curve shown in Figure 4-4.) Figure 4-7 demonstrates the substantial effect that statistical coupling between base and acoustic inputs can have on the random response of structures. Similar effects will be demonstrated for a plate (Section 4.3.4).

4.3.3 Single Point Force Excitation of a Plate

During the development of RAND a number of solutions were run and comparisons made with existing analytical solutions in order to verify Program RAND. For example, RAND results were compared with an analytical solution by Wittig[3] for the mean square velocity of a rectangular, simply supported plate subjected to a random point force having a white noise input spectrum. The results of this comparison are shown in Figure 4-8. The RAND solution utilizes only sixteen degrees of freedom and therefore accounts for a very small portion of the modes included in the analytical solution. Still, however, convergence is rapid and the two solutions are in good agreement. The question of convergence is discussed further in the next section.

4.3.4 Combined Base and Acoustic Excitation of a Plate

Next we consider in more detail a plate response problem where the excitation is more realistic than in the previous example. For this example an aluminum plate is chosen which measures 4 ft. by 3 ft., with a thickness of 0.2 in. This thickness is chosen to insure a fundamental frequency low enough to be affected by the low end of the input spectra. The plate is assumed to be simply supported on all four edges. Modal damping is assigned a

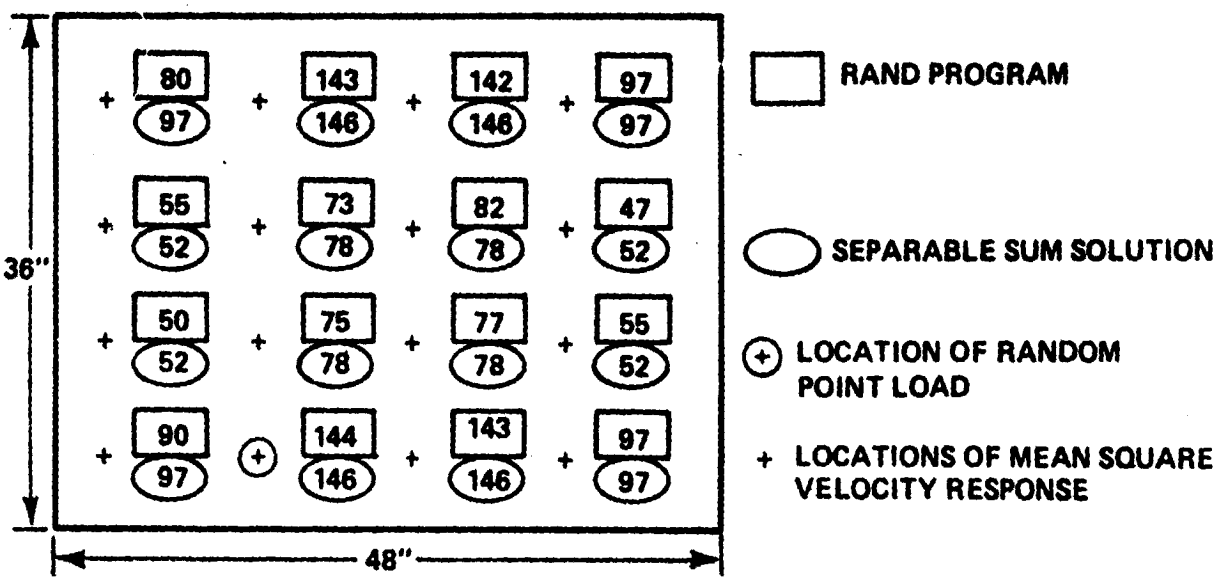

Fig. 4-8 Integrated Velocity Power of Rectangular Plate Driven by Random Point Load Input

value of $\zeta = .05$ for the first mode and assumed to decrease for higher modes so that the product $\zeta\omega_n$ remains constant. Such a plate has sixty-four natural frequencies below 1000 Hz. Only eighteen of these modes participate when excited by either a uniform pressure or a base input. The input spectra ranges in frequency from 30 to 1000 Hz as shown in Figure 4-9.

At first the base and pressure inputs are assumed to be statistically independent. The integrated displacement responses for these independent inputs, computed separately by RAND, are shown in Figure 4-10. Evident from this figure is the fact that the displacement response converges rapidly for both inputs, and is almost entirely determined by the first few participating modes. One can conclude from this that any instrumentation (such as a strain gage) that relies solely on displacement response for input identification would be completely ineffective at mid and high frequencies. Because both inputs are spatially uniform, the response is symmetric and the largest response occurs at the center of the plate. The magnitude of the integrated RMS response due to both inputs is 0.115 in., or approximately one-half of the plate thickness.

The integrated acceleration responses for independent pressure and base inputs are shown in Figure 4-11. They exhibit an entirely different character than the displacement responses in that convergence is not evident. The integrated response increases a little as each participating mode is encountered. Acceleration response data is clearly preferable to displacement response data

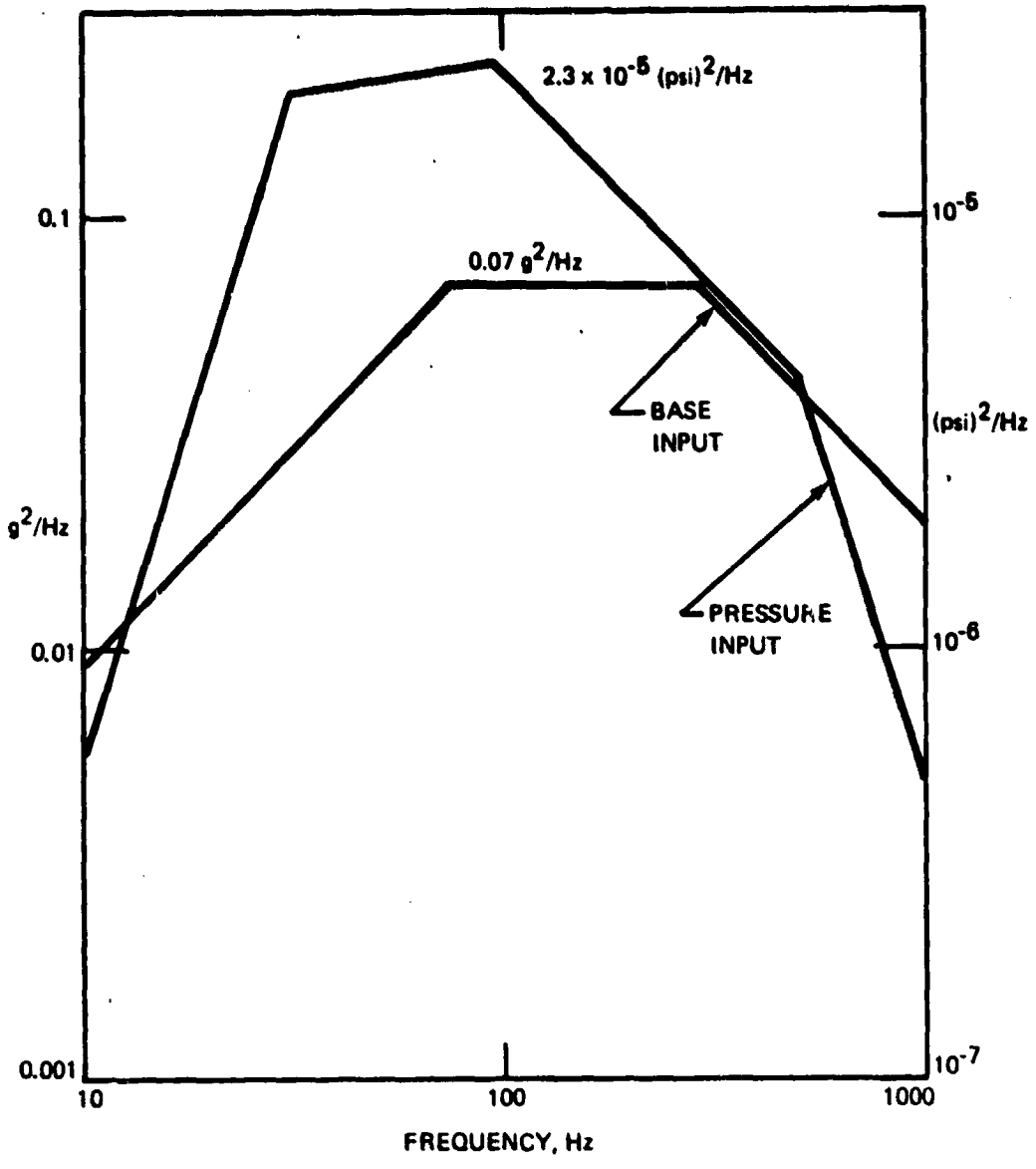

Fig. 4-9 Combined Base and Acoustic Excitations for Plate

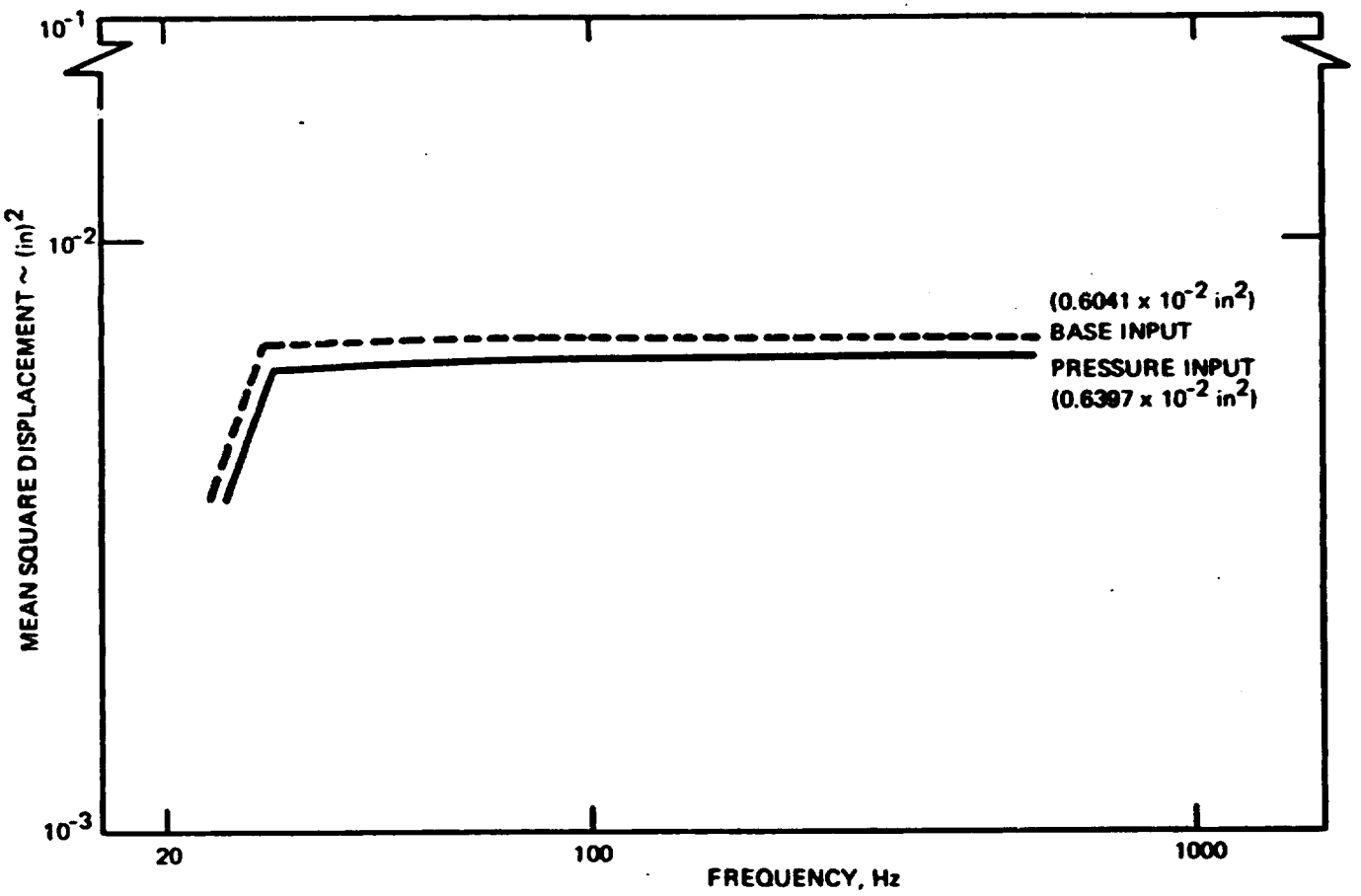

Fig. 4-10 Integrated Displacement Power of Plate for Statistically Independent Base and Acoustic Inputs

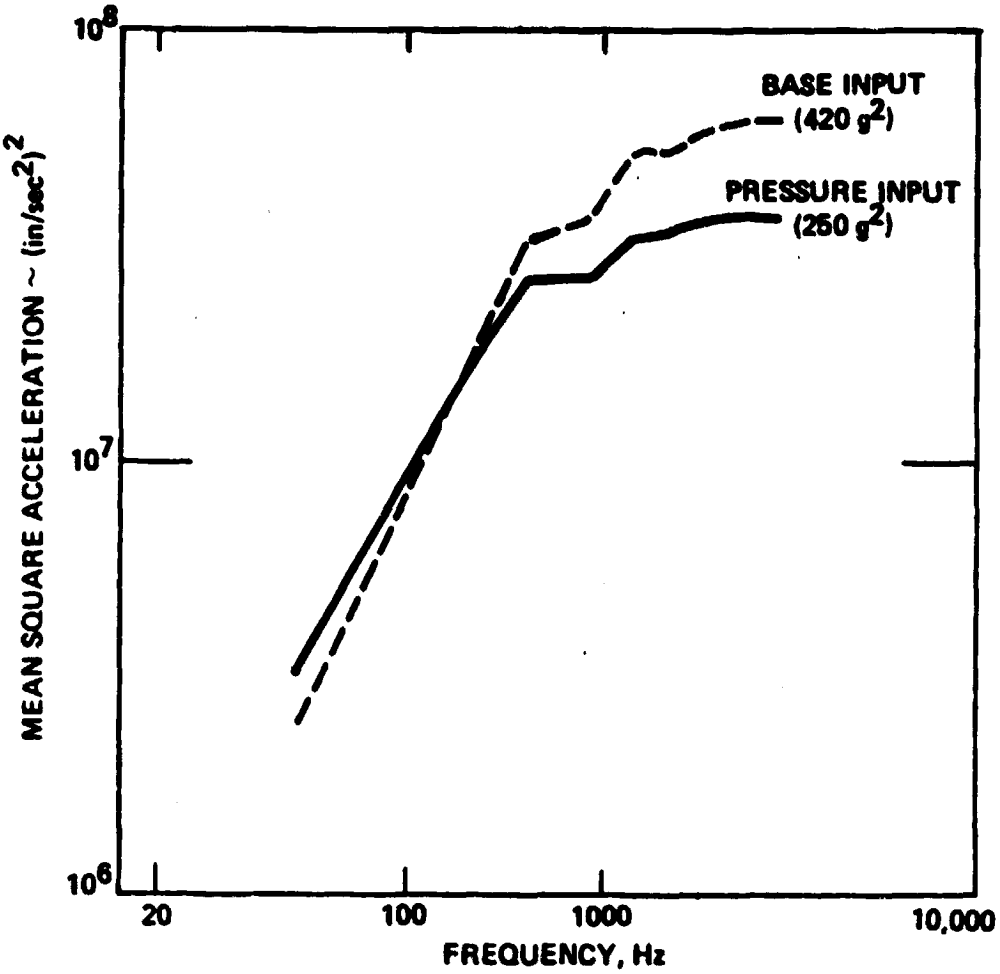

Fig. 4-11 Integrated Acceleration Power of Plate for Statistically Independent Base and Acoustic Inputs

for the identification of inputs over a wide frequency range. The spatial distribution of acceleration over the plate (not shown here) is again symmetric, and indicates that the center of the plate has a higher response by a factor of almost two over any other plate location. This suggests that the center of the plate acts as a collector of energy and is, therefore, the best site for the location of an accelerometer.

The effect of statistical coupling between the base and pressure inputs can be investigated using the same plate model described above. The base and pressure PSD characteristics are chosen to be white noise, their respective power amplitudes sized to cause a roughly comparable response of the plate if applied separately. Fig. 4-12 shows the integrated acceleration response at the center node of the plate for several variations in cross power phase angle ψ and for two values of the coherence ratio (all assumed constant with frequency). Note that the integrated response can range from a low value of 4 g's RMS to a high of 30 g's RMS depending on the phase between the base and acoustic inputs, a result consistent with the simple oscillator study discussed earlier in Section 4.3.1 For a phase angle of 90^0 the response is equal to 22 g's RMS. This value is nearly equal to the response that would occur if the two inputs were uncorrelated. This large range of possible responses is directly attributable to the statistical coupling between the base and pressure inputs, since these inputs have remained unchanged in this plate response example. This emphasizes the need to assess the magnitude and phase characteristics of any statistical coupling between inputs.

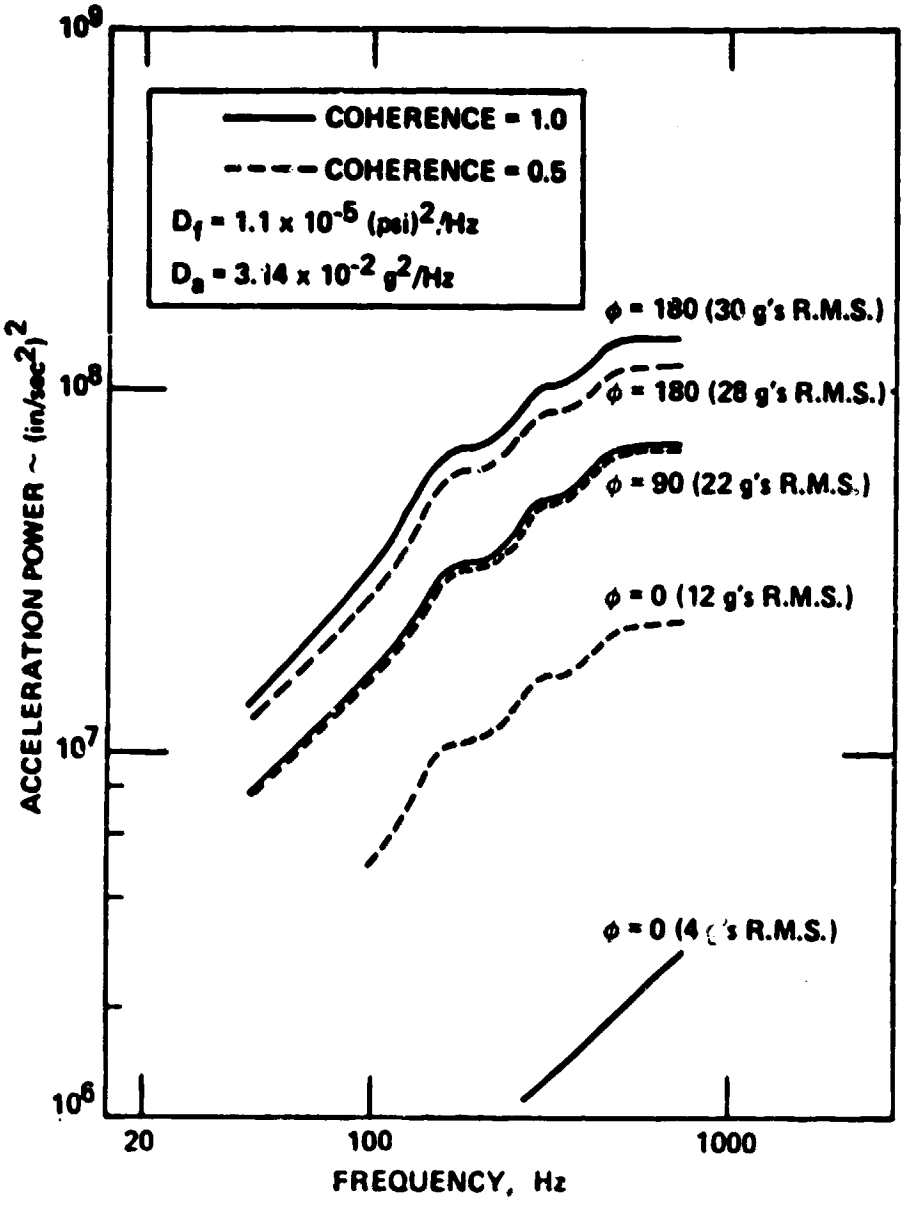

Fig. 4-12 Integrated Acceleration Power of Plate for Combined Inputs with Varied Statistical Coupling

4.4 Parametric Design Guidelines for Plates Subjected to Random Excitation

Parametric relationships for plates subjected to random excitation are developed separately for a pressure input and for a base input. Consider first the forced response of a damped single degree of freedom system of mass M, resonance quality factor Q and natural frequency ω_n. Proportionality relations for the mean square responses for displacement and acceleration are:

$$\text{mean square displacement} \sim \frac{G_f Q}{M^2 \omega_n^3} \tag{4-39}$$

$$\text{mean square acceleration} \sim \frac{G_f Q \omega_n}{M^2} \tag{4-40}$$

where G_f is the input force power spectral density taken to be a constant near ω_n. The response of the single degree of freedom system can serve as a model for the resonant modes of a plate with the exception that the effect of a modal participation factor must be included for each mode. Consider next that the effect of damping and modal participation factor are held constant, and only the plate mass and its natural mode frequencies are varied. The plate mass m is simply

$$m = \rho abt \tag{4-41}$$

where ρ = mass density

a,b = plate length and width

t = plate thickness

The fundamental frequency of the plate is

$$\omega_n^2 = \frac{D}{\rho t} \left[\left(\frac{\pi}{a}\right)^2 + \left(\frac{\pi}{b}\right)^2 \right]^2 \tag{4-42}$$

where D = plate bending stiffness = $\frac{Et^3}{12(1-\nu^2)}$.

As the mass and fundamental frequency of the plate is varied so will the mass and the frequency of each higher mode be varied accordingly. The total response to all the modes will then be a summation of modal responses, each similar to eqn (4-39) for displacement, or eqn (4-40) for acceleration. Parametric relations for the RMS response of the plate are obtained by substituting eqns (4-41) and (4-42) into eqns (4-39) and (4-40), and then taking the square root of the resulting expression. These relations are shown in Table 4-1. The parameters can be divided into three groups representing the effects of plate geometry, plate material, and plate thickness. (η refers to the material loss factor). These groups are represented by the symbols D and A for the displacement and acceleration response respectively, and with the subscripts G, M, and t to denote geometry, material and thickness. Figures 4-13 through 4-17 present plots of the effects of geometry, material and thickness on plate response.

Figures 4-13 and 4-14 show the dependence of the geometric parameters A_G and D_G on the aspect ratio β of the plate for several values of the plate width b. Displacement parameter D_G decreases monotonically with increasing β. In contrast, acceleration parameter A_G reaches a maximum at $\beta = 1.33$ and then slowly decays.

The effect of material selection on displacement and acceleration response is shown in Figure 4-15. The displacement and acceleration parameters D_M and A_M each shows a dependence on modulus E and density ρ which differs greatly from the modulus-to-density ratio commonly used in the design of precision aerospace instruments. As a result such inexpensive metals as steel and brass

Table 4-1 Parametric Relationships for RMS Response of Plate

Pressure Input

$$\text{Disp.} \sim \frac{a^2 b^2}{(a^2+b^2)^{3/2} E^{3/4} \rho^{1/4} t^{5/2} \eta^{1/2}} = \frac{D_G D_m D_t}{\eta^{1/2}}$$

$$\text{Acc.} \sim \frac{E^{1/4} (a^2+b^2)^{1/2}}{a^2 b^2 \rho^{5/4} t^{1/2} \eta^{1/2}} = \frac{A_G A_M A_t}{\eta^{1/2}}$$

Base Input

$$\text{Disp.} \sim \frac{a^2 b^2 \rho^{3/4}}{(a^2+b^2)^{3/2} E^{3/4} t^{3/2} \eta^{1/2}}$$

$$\text{Acc.} \sim \frac{E^{1/4} (a^2+b^2)^{1/2} t^{1/2}}{a^2 b^2 \rho^{1/4} \eta^{1/2}}$$

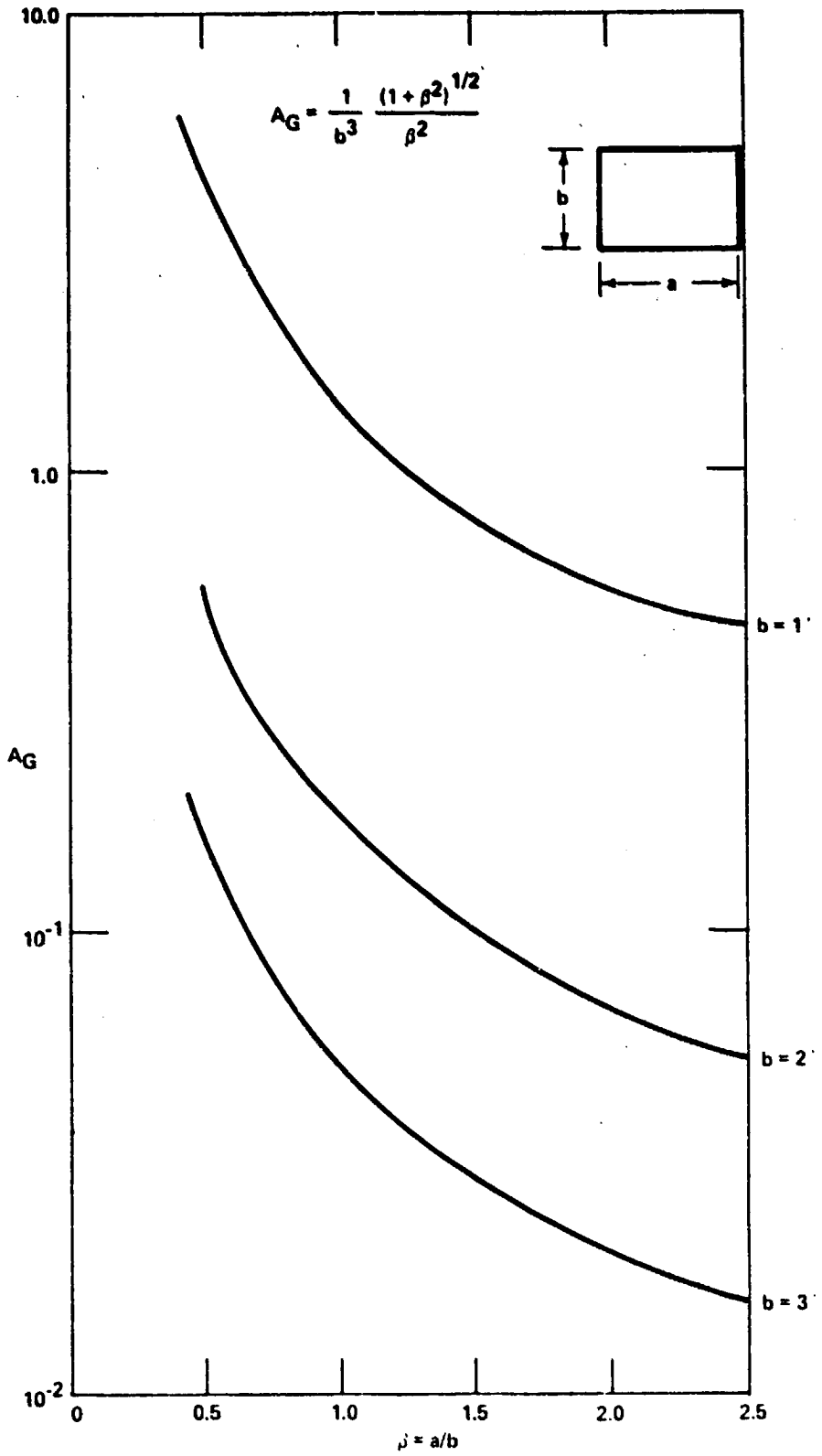

Fig. 4-13 Effect of Geometry on RMS Plate Displacement (Pressure Input)

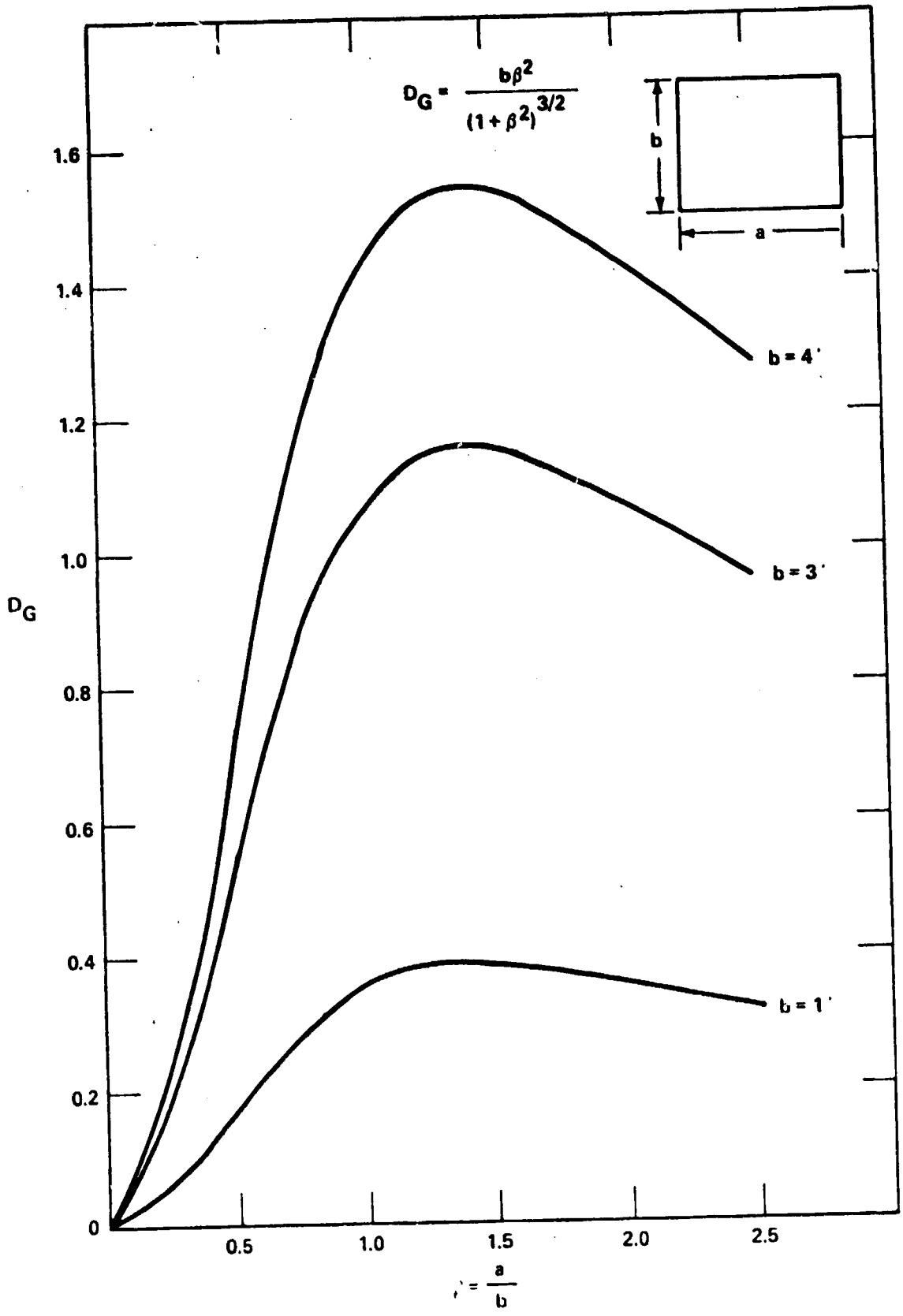

Fig. 4-14 Effect of Geometry on RMS Plate Acceleration (Pressure Input)

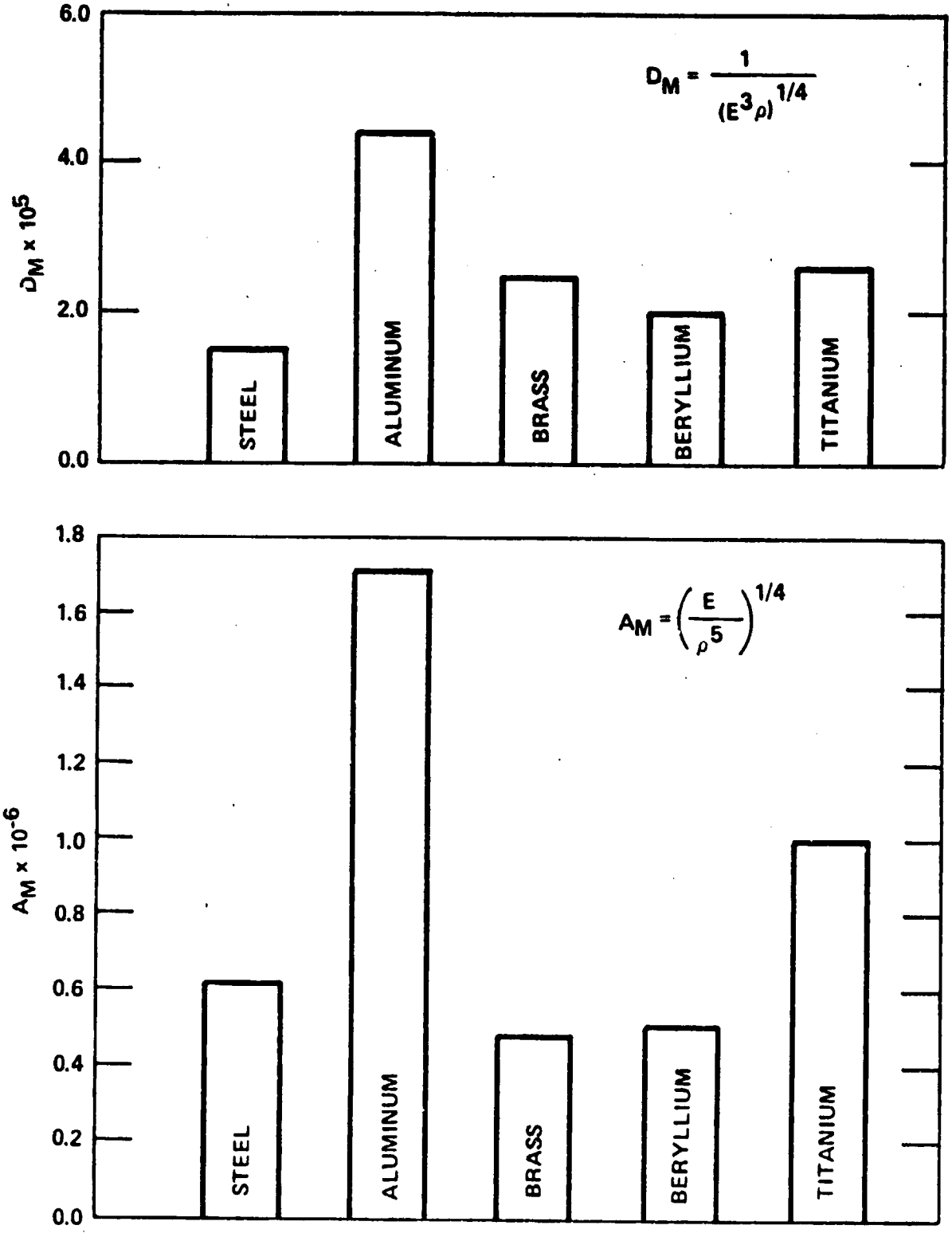

Fig. 4-15 Effect of Material on RMS Plate Response (Pressure Input)

compare favorably with the expensive metal beryllium as far as random response is concerned.

Figures 4-16 and 4-17 show the effect of thickness on response. The effect of thickness on displacement response is very pronounced. In contrast, the effect of thickness on the acceleration response is relatively mild.

All of the parameter effects described above have been verified by RAND. Typically the response of a particular plate can be determined for a given input. The geometry, thickness and maerial properties can then be changed arbitrarily and the new response predicted to within a few percent by using the parametric relationships.

The development of corresponding parametric relationships for base excitation follow the same approach as for the pressure case. In this development there is one major difference: it becomes evident that one can address either the relative or the absolute plate response. RAND studies show that the majority of the response of a plate to a base input is produced by motion of the plate relative to its supports. Using D'ALembert's Principle, the forcing function for this relative response is proportional to the mass per unit area ρt. This suggests that the parameters for base response can be obtained from the pressure response parameters simply by multiplication of the latter by the factor ρt, as shown in the bottom half of Table 4-1. Note that only the geometry parameter is unchanged. Changes in the material and thickness parameters will yield response predictions for the base

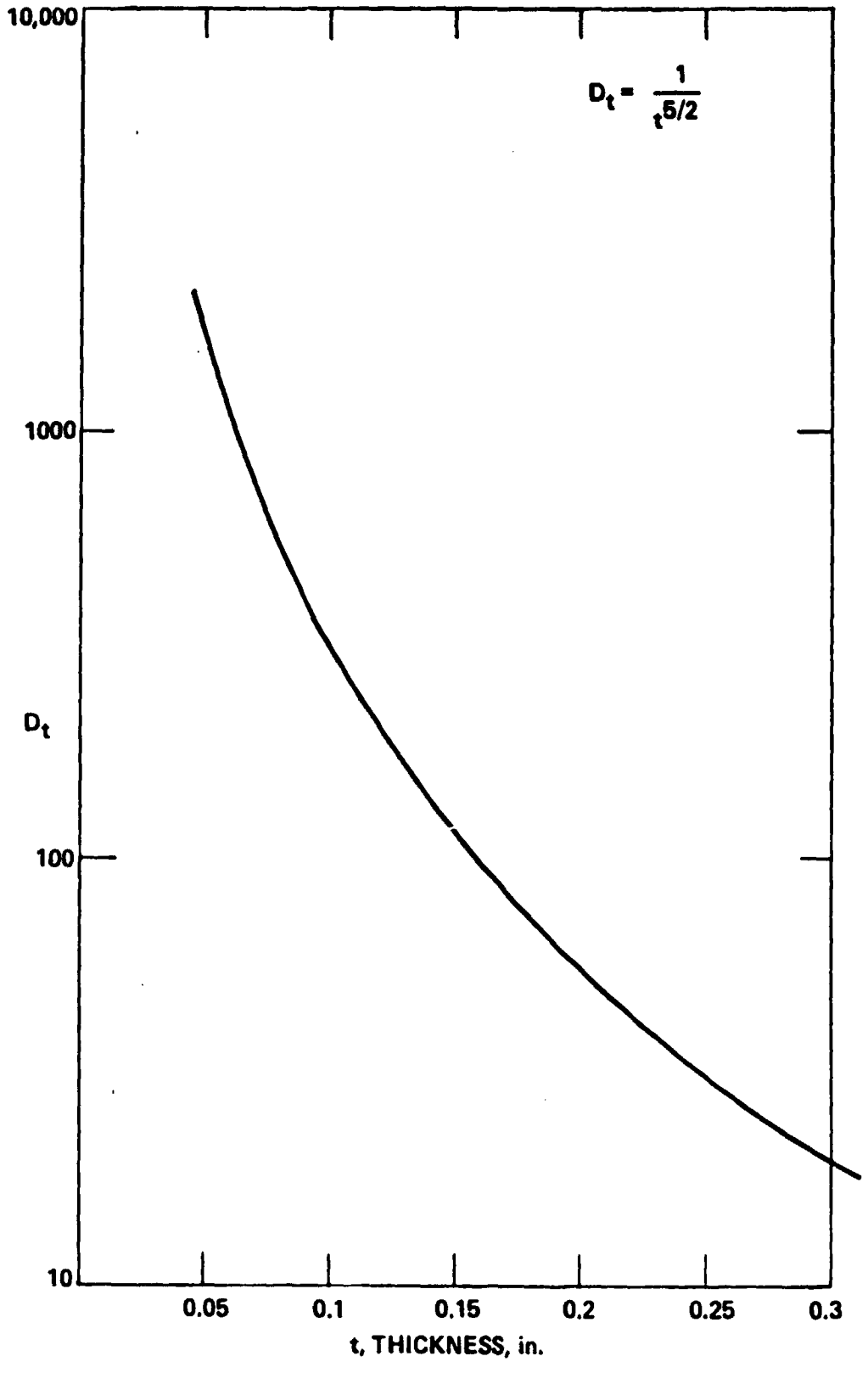

Fig. 4-16 Effect of Thickness on RMS Plate Displacement (Pressure Input)

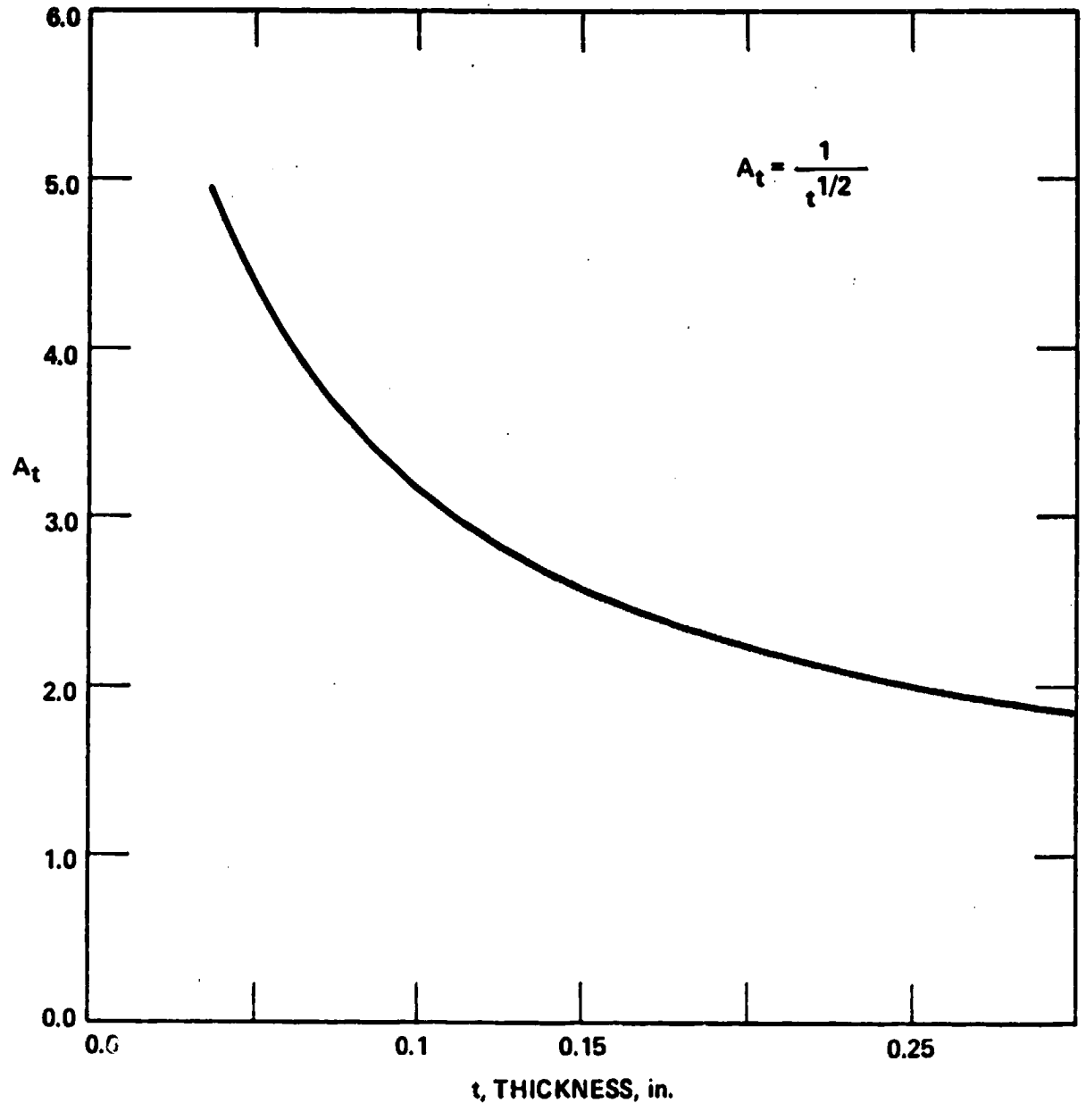

Fig. 4-17 Effect of Thickness on RMS Plate Acceleration (Pressure Input)

input case which differ from the corresponding prediction for pressure input. As before, the accuracy of these base response parameters have been verified by Program RAND.

The purpose of this parametric study was to develop the ability to predict changes in response due to changes in structural configuration and as a result to be able to predict the response of a newly designed plate by comparing its physical characteristics to a plate with a known response. The above parametric relationships accomplish this goal.

4.5 Conclusion to Part I

Program RAND is a practical and useful tool for making response and input identification estimates for any multi-degree-of-freedom structure subjected to both base and acoustic inputs. Displacement response computations, suitable for stress and sway space estimates, converge quickly and require only a low frequency representation of the structure. On the other hand, acceleration response computations, suitable for the estimation of g loads and for designing subassembly tests, do not converge quickly. In the latter case, the structural model must have good fidelity over a bandwidth which includes all frequencies of significant excitation. In the case of an acoustic input this bandwidth may extent to 10 KHz.

Practical limitations to the RAND estimation procedure do not relate to the program itself, but rather to the program inputs. The limited fidelity of the finite element model used to characterize the structure has already been mentioned. A second input limitation, looking ahead to Part II of this study, results from

the difficulty of accurately measuring the random base or acoustic excitations. As far as model fidelity is concerned, perhaps a reasonable approach is to use Program RAND for low frequency displacement studies, and for acceleration studies up to mid frequency range. Truly high frequency problems will probably best be studied using the technique of Statistical Energy Analysis. Input accuracy limitations are discussed in part II.

5.0 Part II: Experiment-Based Models for Structural Response and Input Identification

5.1 Introduction to Part II

In describing the experimental portion of this study a distinction has been made between low resolution and high resolution experiments. This distinction reflects the historical fact that originally only a low resolution Fast Fourier Transform (FFT) analyzer was available for use in this study. Subsequently a high resolution capability was added to the analyzer. Although the low resolution results are in some respects inferior in quality to the high resolution results, there are advantages and disadvantages associated with both types of measurements. Consequently there is much to be learned by contrasting the low and high resolution measurements, and they have been given equal emphasis in this report.

5.2 Laboratory Test Description

A simple schematic of the test set up for combined base and acoustic inputs is shown in Figure 5-1. The corresponding instrumentation layout is shown in a more detailed fashion in Figure 5-2. With this equipment it was possible to excite the plate by a base input, by an acoustic input, or by combined base and acoustic inputs. Note that in the combined input case both the base and acoustic excitation are caused by the same source, namely the MBT495 Random Noise Generator. This means, of course, that the base and acoustic inputs are fully correlated statistically, and the nature of the cross power spectral density between these excitations is wholly determined by the frequency transfer characteristics of the base and acoustic channels which exist between the noise source and the aluminum plate.

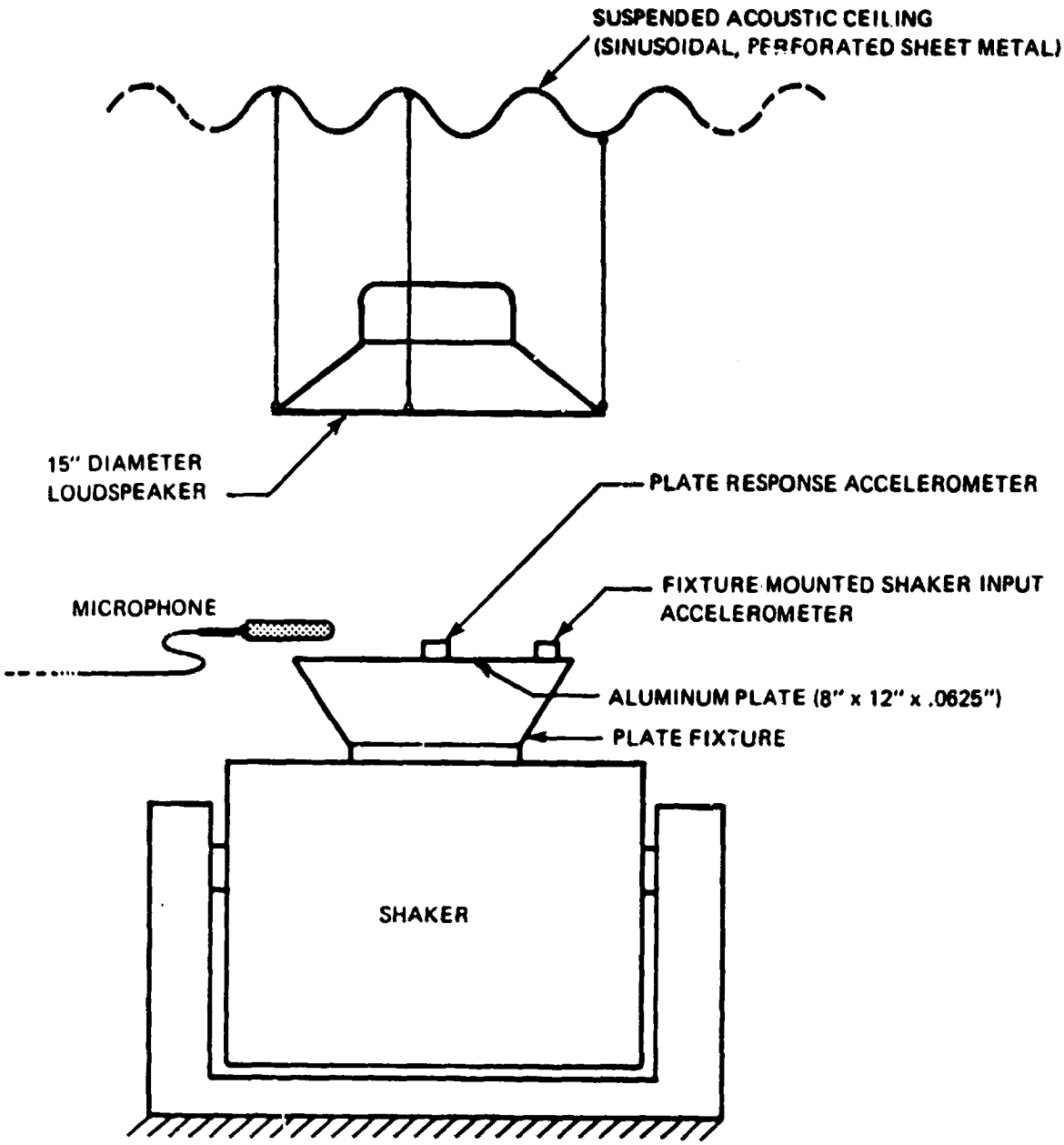

Fig. 5-1 Test Set Up: Combined Base and Acoustic Input

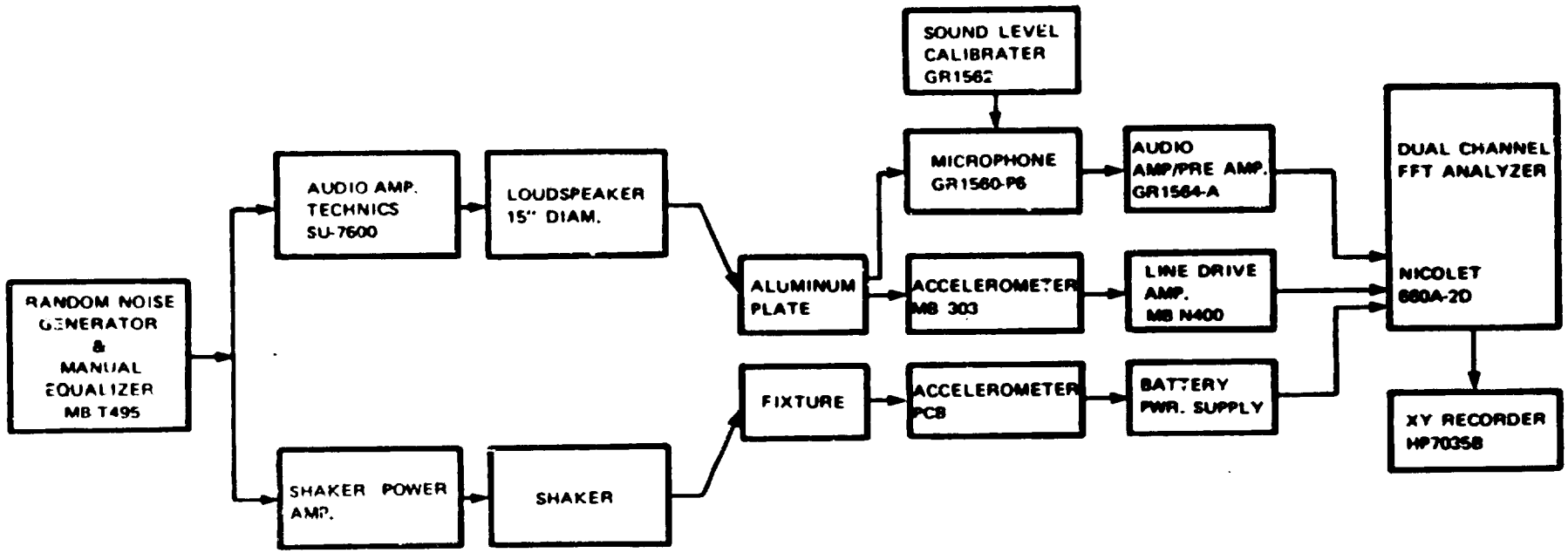

Fig. 5-2 Instrumentation Lay-Out

In the experiments the procedure was to measure input and response spectra under various conditions of excitation and then to compare these spectra with those predicted by Program RAND. In order for RAND to be executed it is necessary to specify the dynamic modal parameters of the plate. The required parameters are the modal damping ratio vector ζ, the modal frequency vector f and the mode shape matrix U. Modal damping ratios can only be determined by experiment, and much effort was expended in this study attempting to obtain reliable damping estimates. On the other hand, frequency and mode shape estimates can either be made experimentally or by the use of a computer-aided finite element analysis. Probably the preferred approach is to determine these parameters wholly by experiment, since no idealized assumptions are required as with the finite element modelling process. And with the availability of computer-based modal analysis systems the experimental approach may also be easier. Unfortunately in this study no such modal analysis system was available. Mode shape estimates were therefore based on a finite element analysis using Program SAP IV. Damping and frequency data was obtained experimentally.

The question of boundary conditions requires special attention. The analytical approach embodied in Program RAND utilizes the principle of linear superposition, and the ideal assumption is made that a base input, of infinite source impedance, acts independently of the acoustic input, which has zero source impedance. The experimental reality is rather more complex. As will be detailed below in the treatment of input loading effects, both the shaker and the

loudspeaker possess a finite source impedance. Further, these inputs are dynamically coupled: for instance, the base input level, as measured by the plate fixture accelerometer will be caused to change merely by turning on the acoustic input. The RAND assumptions are still valid and the RAND predictive procedure is still applicable to real structures; it is just that particular care must be taken concerning boundary conditions in a test situation. Consider for example that we want to compare RAND predictions with experiment for the case of acoustic input only. Since the analytical approach assumes infinite source impedance for the base input and, in this case, the base input amplitude is assumed to be zero, the proper experimental procedure is clearly to mechanically block the shaker input. Alternatively, a pure base input test, without any acoustic interaction, would require removing the loudspeaker, or, better yet, to remove any acoustic effects by operating in a vacuum. The difficulty with boundary conditions occurs only when it is desired to test one input at a time. Practically speaking, there will always be combined inputs in a field situation, and the RAND procedure will rigorously apply.

Finally, we consider the question of data averaging. Whereas the analytically derived spectra produced by the RAND predictive procedure have in effect already been averaged mathematically, the experimental data produced by the base input and plate response accelerometers and by the microphone vary randomly, and must be sufficiently averaged to reduce the amount of statistical variation to acceptably small levels. A figure of merit for the adequacy of

this averaging is the confidence level as measured by the equivalent degrees of freedom of the chi-square distribution model of the sampling process. Although the question of confidence level was addressed in these experiments it was not systematically monitored and is not reported on here. A second figure of merit which indicates the quality of data estimates is the coherence ratio. This parameter is related to the signal-to-noise ratio of the data, and is conveniently available on the FFT Analyzer. It was consistently monitored during all tests. A brief review of the coherence ratio follows.

A common situation which arises in structural vibration measurement, which we shall refer to as output noise contamination, is shown in Figure 5-3.

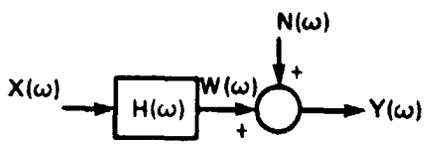

Figure 5-3 Output Noise Contamination

In the Fourier domain, a linear dynamical structure, characterized by its transfer function $H(\omega)$, receives an excitation $X(\omega)$ and responds at a level $W(\omega)$. An independent noise source of strength $N(\omega)$ is present at the output. Define the coherence ratio γ^2 as

$$\gamma^2 = \frac{G_{xy}\, G_{yx}}{G_{xx}\, G_{yy}} \qquad (5\text{-}1)$$

where $G_{ij}(\omega)$ refers to the usual one sided power spectral density. Eqn (5-1) can be rewritten as:

$$\gamma^2(\omega) = \frac{1}{1 + G_{nn}/G_{ww}} \tag{5-2}$$

with $0<\gamma^2<1$ as $\infty>G_{nn}/G_{ww}>0$.

Similarly, noise contamination is possible at the input as shown in Figure 5-4.

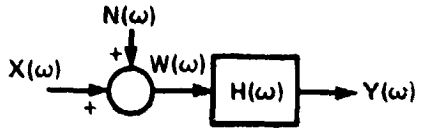

Figure 5-4 Input Noise Contamination

Under the same assumptions, the coherence ratio is

$$\gamma^2(\omega) = \frac{1}{1 + G_{nn}/G_{xx}} \tag{5-3}$$

with $0<\gamma^2<1$ as $\infty>G_{nn}/G_{xx}>0$.

Both input and output noise contamination occurred during the experiments and will be discussed further below.

5.3 Low Resolution Experiments

5.3.1 Modal Damping Ratio Estimates

Early damping measurements were made in the frequency domain using an FFT analyzer which possessed only a base band capability. Base band refers to the bandwidth of a spectrum which extends from zero frequency to a selectable upper frequency. The nominal frequency resolution of the analyzer is then the base bandwidth

divided by the number of spectral lines provided by the particular analyzer configuration. Nominal resolution for the 400 spectral line analyzer (in base band operation) is given in Table 5-1 as a function of base bandwidth setting.

Base Bandwidth Setting	Nominal Frequency Resolution
0 - 500 Hz	1.25 Hz
0 - 1000 Hz	2.5 Hz
0 - 2000 Hz	5 Hz

Table 5-1 Frequency Resolution for Baseband Operation

As an example, low resolution estimates of the quality factor Q_1 of the first plate mode (f_1=240 Hz) varied from $25<Q_1<100$ depending on base band setting. The actual Q of the first mode, determined later by using an analyzer with a digital frequency expansion (Zoom) capability, was about 109. The actual half power bandwidth of the first mode is therefore about $\frac{240}{109}$ = 2.2 Hz. Clearly none of the above base bandwidth settings (Table 5-1) can adequately resolve the sharp resonance peak of the first plate mode.

Time domain estimates of damping ratio were also attempted. The log decrement of the transient decay envelop of the plate were measured after passing the plate response signal through a band pass filter centered at the particular mode frequency of interest. Damping estimates were improved by this technique. For example, the first mode quality factor ranged from 76<Q<89. The method proved, however, to be tedious and inconvenient. It was also suspect

from a theoretical point of view: the plate dynamic characteristics were being windowed by the electronic filter which possessed its own dynamic characteristics.

The proper estimation of damping is crucial to the success of any scheme of structural response or input identification estimation. And proper estimation of damping requires the use of instrumentation which has adequate resolution. It will be shown below in this report that there are certain advantages to making low resolution measurements of the input and output spectra in structural dynamic studies. The requirement of high resolution measurements for damping, however, remains unchanged.

5.3.2 Excitation and Response Spectra

Typical examples of low resolution excitation and response spectra for the plate are shown in Figure 5-5, for the case of base input, and in Figure 5-6, for the case of acoustic input. In both cases a broad band input excitation extends from nearly zero to 2000 Hertz. The five major peaks in the plate response spectra correspond to five participating normal modes predicted by a combined SAP IV and RAND analysis, as shown in Table 5-2.

SAP Mode Number	SAP Resonant Frequency	RAND Participation	Experimental Resonant Frequency
1	252.2 Hz	X	250 Hz
2	391.1		
3	622.8		
4	626.7	X	605
5	755.5		
6	954.6		
7	981.2		
8	1192	X	1105
9	1300		
10	1324		
11	1373	X	1310
12	1545	X	1445

Table 5-2 Comparison of Finite Element (SAP) and Experimental Mode Frequencies

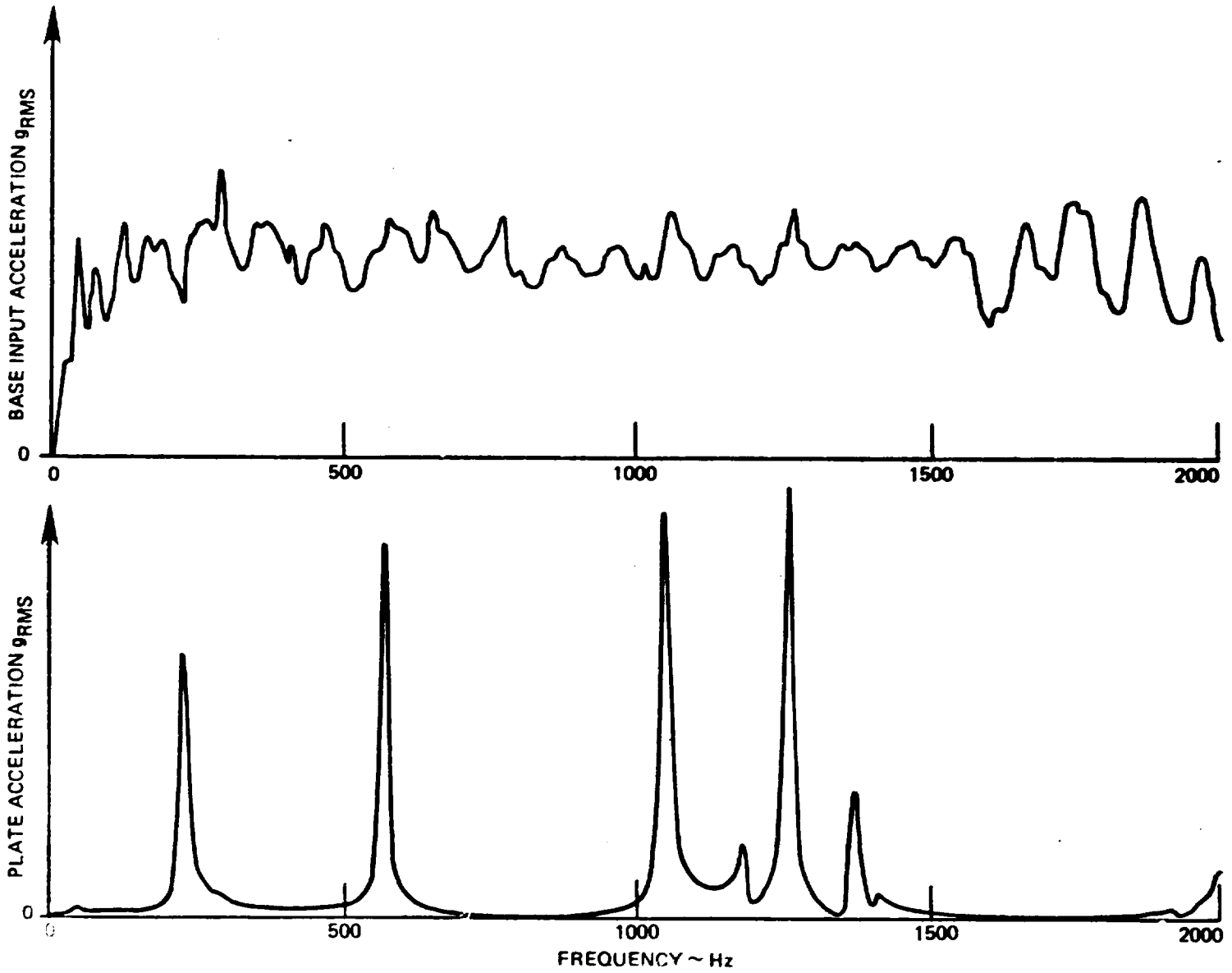

Fig. 5-5 Low Resolution Spectra: Plate Response to Base Input

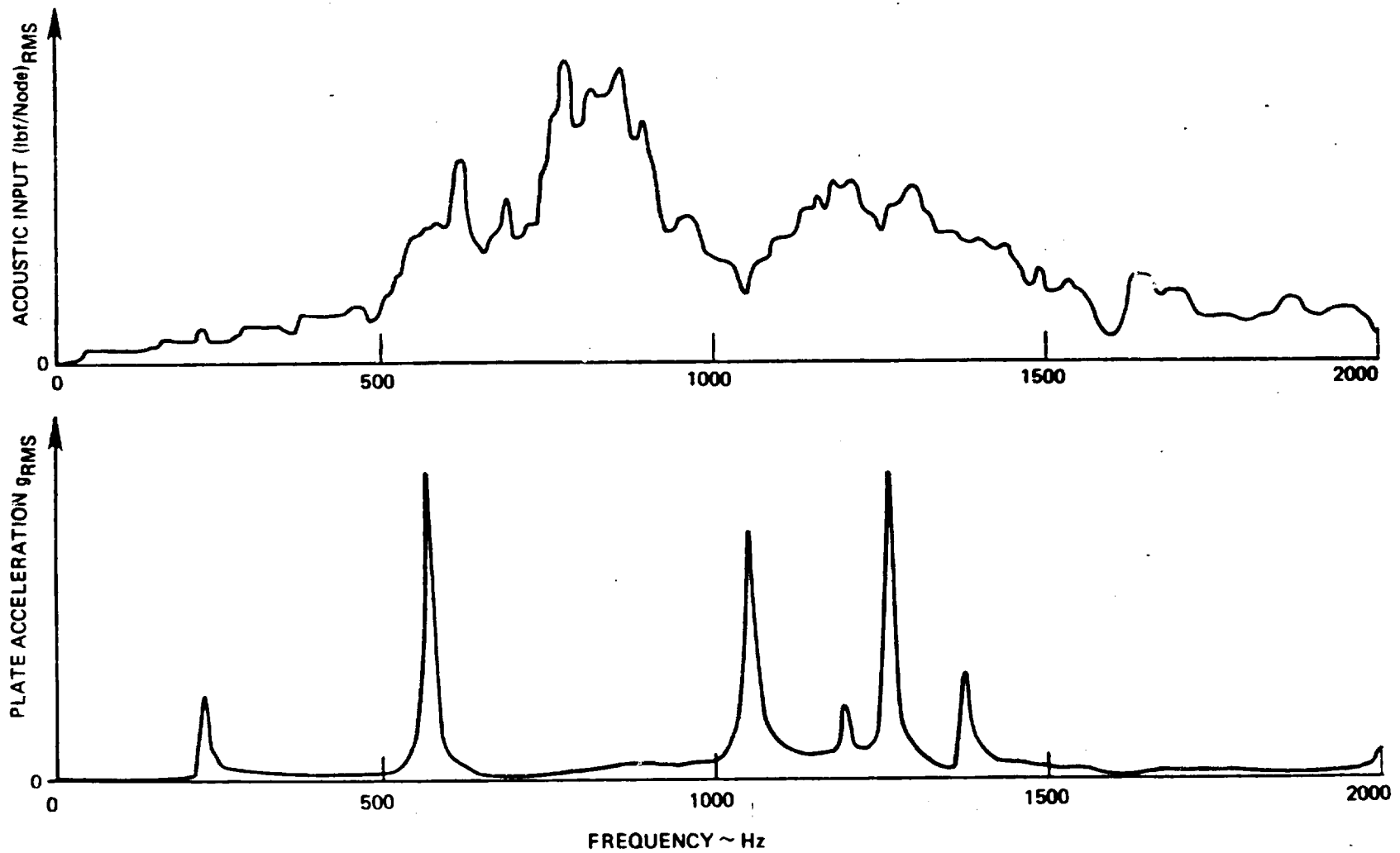

Fig. 5-6 Low Resolution Spectra: Plate Response to Acoustic Input

The SAP IV finite element model has yielded frequency estimates which are acceptably close to the experimental values, although the question of accuracy of the finite element model is not an important issue, since we have already pointed out that the modal parameters (frequencies, damping ratios, and mode shapes) are best obtained experimentally using modal analysis equipment. Note that a spurious small response peak occurs at approximately 1200 Hz. This was not predicted by the combined SAP/RAND analysis and was not included as a transfer characteristic of the plate in any subsequent RAND response predictions or input identifications. Again, were modal analysis equipment available, this response detail would be routinely incorporated in the plate model representation of Program RAND.

We turn now to the question of the quality of these spectra estimates. As stated above, the spectra have been sufficiently averaged timewise to the point of negligible statistical variation. However, a plot of the coherence ratio, shown in Figure 5-7, indicates that the signal-to-noise ratio is sharply reduced at a number of critical frequencies. In this Figure the base excited plate response is presented as a semi log plot to allow study of regions of very large resonant response as well as regions of very low antiresonant response. Resonant and antiresonant responses are most easily described analytically in terms of the poles and zeros of the transfer function, which can in general be written in the form

$$H(s) = \frac{k(s-z_1)(s-z_2)\text{---}}{(s-p_1)(s-p_2)\text{---}} = \frac{kZ(s)}{P(s)} \qquad (5\text{-}4)$$

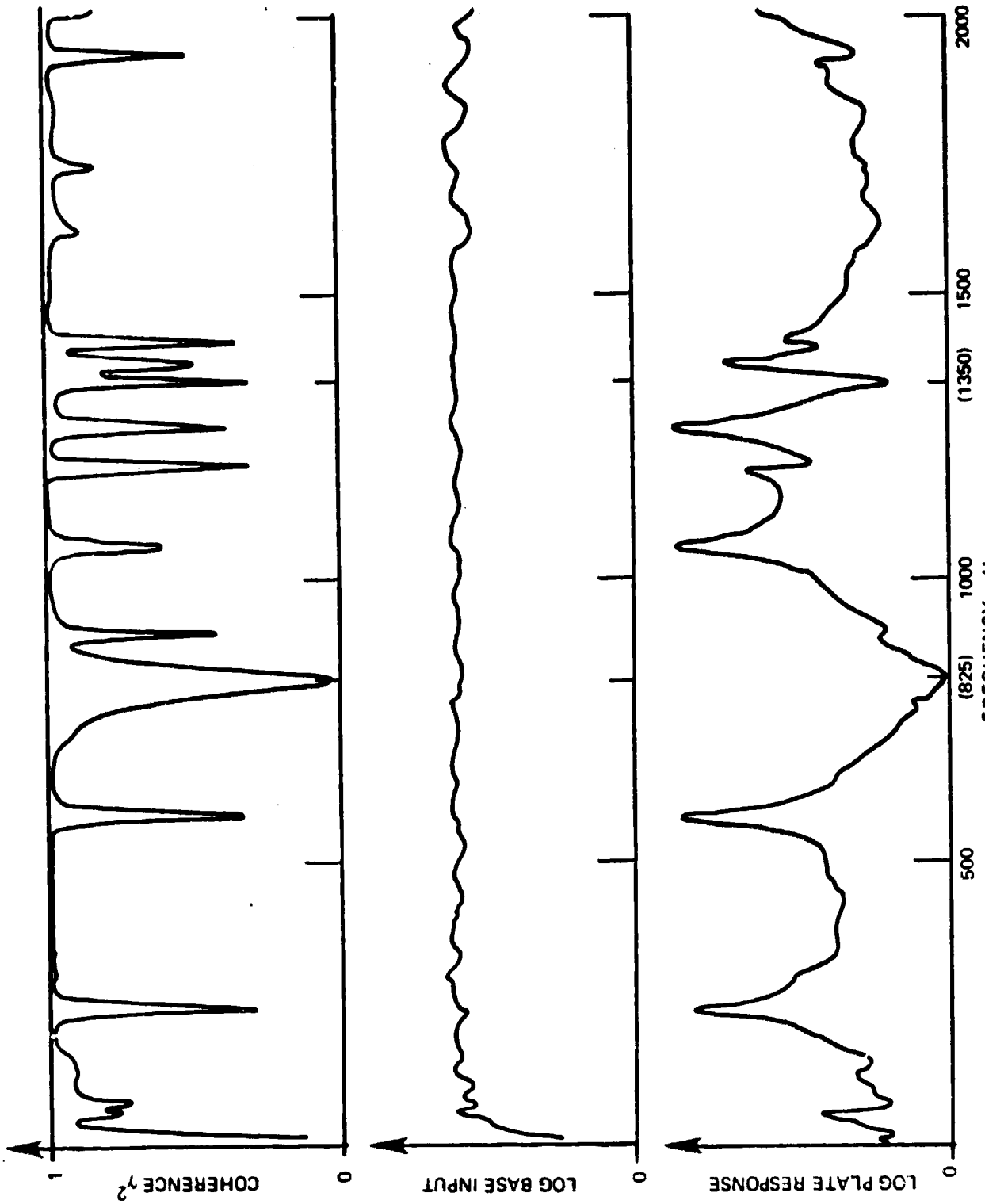

Fig. 5-7 Low Resolution Base Input and Response Spectra for Plate (Semilog plot)

where the transfer function zeros z_1, z_2--- are roots of the equation $Z(s) = 0$, and the transfer function poles p_1, p_2--- are roots of the characteristic equation $P(s) = 0$. For very lightly damped structures these poles and zeros occur in conjugate complex pairs which are located very near to the imaginary axis. The plate response spectrum PSD $G_p(\omega)$ is related to the base input spectrum $G_b(\omega)$ by the equation

$$G_p(\omega) = G_b(\omega) \, |H(\omega)|^2 \qquad (5\text{-}5)$$

where $H(j\omega)$ is the frequency response function obtained from the transfer function $H(s)$ simply by setting $s=j\omega$. A resonance occurs when $|H(j\omega)|^2$ is maximum. This in turn occurs when the value $s=j\omega$ is very close to (effectively is equal to the imaginary part of) a transfer function pole p_1, p_2--- etc. Similarly an antiresonance occurs when $|H(j\omega)|^2$ is a minimum. This in turn occurs when the value $S=j\omega$ passes very close to (again, effectively equals the imaginary part of) a transfer function zero z_1, z_2--- etc. A resonance is a global characteristic of the structure and exists independently of the spacewise nature of the input. An antiresonance, on the other hand, is a local characteristic of the structure; that is, it applies to a particular location only. Further, the location of the antiresonance, both spatially and in frequency, depends on the spatial distribution of the input excitation.

Consider now the two antiresonant responses which occur approximately at 825 Hz and at 1350 Hz as shown in Figure 5-7. Since the damping of the structure is very small, the antiresonant response is also very small (zero damping would result in truly a zero

response). Clearly such a small signal will be corrupted by ever present background noise. Hence a sharply reduced value of the coherence ratio. Since this noise contamination occurs at the output (response) of the transfer function $H(\omega)$ we have an example of output noise contamination as shown in Figure 5-3.

Significant reduction in the coherence ratio also occurs at the resonant frequencies. However, the mechanism for this - an input noise contamination caused by input loading effects - is obscured in this data because of inadequate resolution of the FFT. The details of the input loading phenomenon will be taken up later during the discussion of the high resolution experiments.

5.3.3 Response Prediction Using Program RAND

At this point an attempt was made to compare the plate response level obtained experimentally with the same response level predicted by Program RAND. The RAND model of the plate used damping ratios determined by free vibration decay measurements, natural frequencies obtained by FFT measurement, and mode shapes obtained by finite element analysis. Four separate experiments were conducted using base input excitation only. The base input and plate response spectra were measured using the low resolution FFT analyzer. Because the FFT analyzer could not resolve the sharp response peaks adequately, there was little hope that experimentally measured response spectra would agree with the corresponding spectra predicted by RAND. However, FFT measurements of the rather slowly varying broad band input spectra could be expected to be fairly good. And the integrated area of the response peaks, that is, the

overall power of each resonance, would also be fairly accurate because the FFT algorithm accurately computes the correct power of the time windowed signal, independent of resolution adequacy. The results of these four runs are given in Table 5-3. The agreement between experiment and Program RAND is rather satisfactory, particularly when it is remembered that the excitation data input to RAND suffered from noise contamination and the input spectrum was poorly resolved. Reasons for the relative success of the prediction procedure in the presence of these error producing effects will be discussed later after the high resolution results have been presented.

Run No.	Total Overall Response		
	Experimental	Program RAND	Error
1	40.4 g^2	44.8 g^2	+.45 dB
2	41.1	35.2	-.67
3	54.3	40.9	-1.2
4	48.1	37.3	-1.1

Table 5.3 Plate Response Estimates: Base Input, Low Resolution Spectra

5.3.4 Input Identification Using Program RAND

The input identification mode of Program RAND takes as input data the response spectrum of a structure, accounts for the transfer characteristics of the structure, and then computes the spectrum of the excitation applied to the structure. The use of a low resolution FFT analyzer for input identification mode measurements will not be satisfactory since the analyzer must resolve the details of a response spectrum which consists of many sharp resonant peaks.

Nevertheless, it is instructive to look at an early example of an input spectrum identification provided by the RAND procedure using data obtained by the low resolution FFT analyzer, shown in Figure 5-8. A comparison with the actual input spectrum (not shown) shows that the input spectrum estimate is of poor quality as anticipated, particularly near the resonant frequencies at 250 Hz, 605 Hz, 1105 Hz, 1310 Hz and 1445 Hz. But the most important aspect of this spectrum estimate is that it is dominated by three peaks which are very obviously in error, since the actual spectrum was relatively flat with frequency. The presence of these peaks has nothing to do with the low resolution of the FFT analyzer. The first two peaks, at 825 Hz and at 1350 Hz, are caused by the poor signal-to-noise ratio at the two antiresonances described above in Section 5.3.2. At an antiresonant frequency the transfer characteristic of the structure decreases nearly to zero. The structural response, as measured by an accelerometer and estimated by an FFT analyzer, does not decrease nearly to zero (as it should theoretically, and as Program RAND expects) because of the presence of noise. The only explanation for this non-vanishing response, as far as Program RAND is concerned, is that the input must have a very sharp peak. Thus erroneous peaks will always appear in the input identification estimate at each antiresonant frequency of the structure. From a practical point of view the antiresonance-induced error can be avoided by simply instructing Program RAND to set the input identification estimate to zero for a small band of frequency about each antiresonance, a process called blanking.

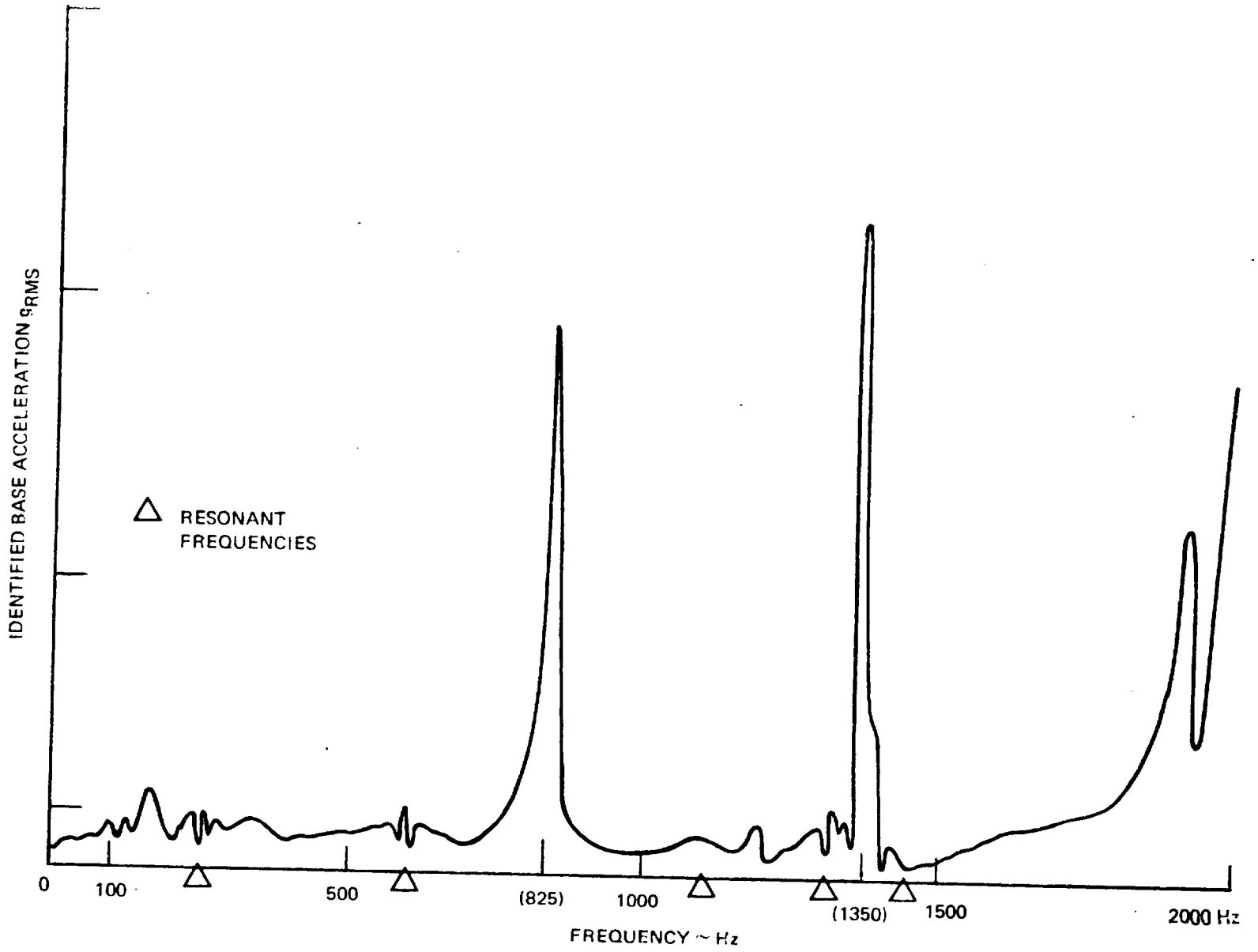

Fig. 5-8 Low Resolution Identification of Base Input to Plate

The implication of this phenomenon is that the transfer characteristic of the structure which is stored in RAND must explicitly include antiresonant frequencies as well as resonant frequencies. It is also clear that the input identification procedure will break down in the region of an antiresonance, and that a portion of the input spectra will be lost because of an inadequate signal-to-noise ratio.

The third large source of error in Figure 5-8 extends over a band of frequency $1800<f<2000$ Hz. This is caused by the fact that the transfer characteristic stored in Program RAND includes only five modes and is therefore only representative of the structure out to a frequency of, say, 1600 Hz. The error can be removed by simply including an additional (sixth) mode, thereby extending the fidelity of the transfer characteristic to 2000 Hz.

The problems described in this section were discovered during early low resolution input identification runs, and they called attention to the importance of assuring adequate bandwidth for the structural transfer characteristic and to the value of antiresonant frequency blanking. These refinements were routinely incorporated in all subsequent low and high resolution studies.

5.4 High Resolution Experiments

5.4.1 Improved Estimates of Damping Ratio and Frequency

The addition of high resolution capability to the FFT analyzer quickly led to damping ratio and resonant frequency estimates which were reproducible and also independent of any further reduction of the resolution bandwidth setting of the analyzer. With this capa-

bility for precision it soon became apparent that the damping ratios and resonant frequencies were affected by subtleties in the boundary conditions of a particular test: for instance, whether or not the shaker fixture was blocked, what type of excitation was used, and whether or not the loudspeaker was in position over the plate. The variation in frequency with changes in boundary condition were typically less than 1%. Unfortunately, due to input loading effects, such small variations in frequency are still significant as far as structural response and input identification estimates were concerned. Discussion of the effect of boundary conditions will be postponed until after an examination of input loading models has been made.

Representative results for high resolution frequency and damping ratio are given in Table 5-4. The tabulated values are based on the base input transfer function obtained by dividing the plate response (at center node) by the base input (at plate fixture). Theoretically (and experimentally) these results are the same as for the boundary condition case in which the fixture motion is blocked.

Mode Number	Resonant Frequency	Damping Ratio	Q
1	239.2 Hz	.0046	109
2	575.5 Hz	.0022	227
3	1050.3 Hz	.0024	208
4	1260.5 Hz	.0015	333

Table 5-4 High Resolution Mode Frequencies and Damping Ratios

These damping ratios are significantly lower (and the corresponding Q values higher) than values obtained previously by low resolution FFT analysis or by the time domain transient decay technique. Once more we emphasize that adequate frequency resolution is essential to the attainment of realistic damping estimates.

5.4.2 Input Loading Effects: Base Excitation

5.4.2.1 First Mode Input and Response Characteristics

High resolution dynamic characteristics of the first mode obtained from a random base excitation test are shown in Figure 5-9. Several features are of interest. First, the base input (curve a) shows a sharp decrease and subsequent increase in level as the plate response peak (curve b) is passed. The input minimum is substantial enough to cause the coherence ratio (curve c) to decrease, showing that the input minimum is contaminated by noise. Curve d shows the phase characteristic of the transfer function $H(\omega)$: specifically, the phase of the plate response lags behind the base input phase by 90^0 at a frequency of 238 Hz. Finally, the magnitude of the transfer function (curve e) reaches a maximum at the same frequency. Note that this frequency differs from the frequency at which the plate response magnitude is a maximum. This pattern, or a similar pattern, rather generally occurred at each structural resonance under both base excitation or acoustic excitation. The pattern consists of a decrease in the input level attended by a decrease in the coherence ratio, also an increase in the input level, and a response maximum which occurs at a frequency which differs from the frequency of maximum transfer function magnitude.

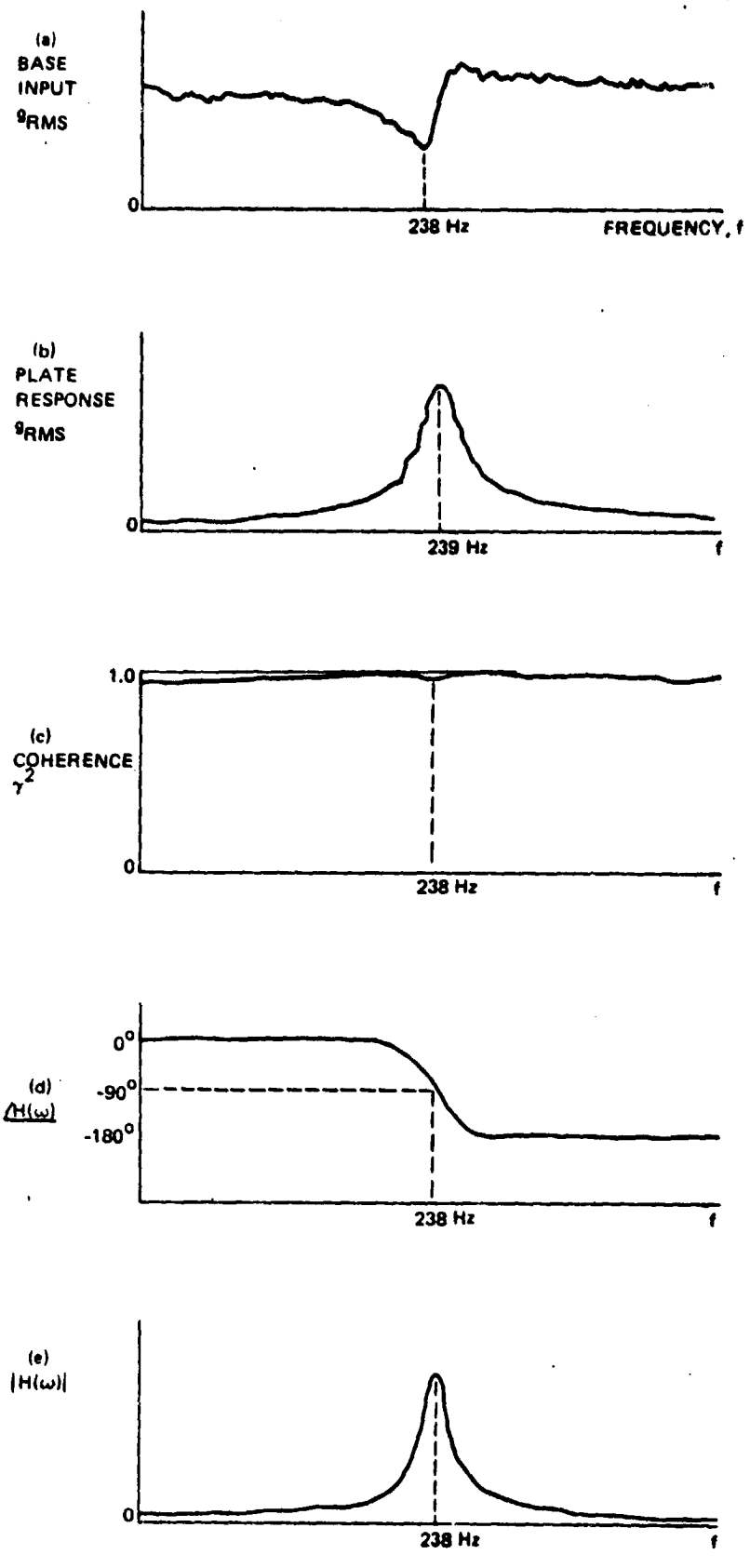

Fig. 5-9 High Resolution Spectra: Plate Response to Base Input (First Mode)

This input loading effect is not a new phenomenon. Much attention was given to input loading in the early days of vibration testing by the designers of electrodynamic shaker systems[4]. In fact, since the loading phenomenon was considered an undesirable feature of vibration testing, electronic compensators called peak-notch filters were developed to render the vibration input spectrum flat with frequency. More extensive need for input spectrum adjustment led to the development of manual and finally automatic compensation devices known as equalizers.

Our interest here in the input loading phenomenon stems from the expectation that input loading should be a relatively common occurrence in field studies of real structures. The value of analyzing the details of the input loading phenomenon in the relatively simple laboratory set up of this study is the insight that it provides for the more complicated field system.

5.4.2.2 Model Development for Input Loading Analysis

As stated earlier, the input loading is caused by the fact that the base and the acoustic inputs possess finite source impedance. Consequently, the base input model must include a real displacement source of finite impedance rather than an ideal displacement source with infinite impedance. Similarly, the acoustic input must be modelled as a real force source of finite impedance rather than an ideal force source of zero impedance. A simple model which adequately explains the input loading effects experimentally observed at the first plate resonance is shown in Fig. 5-10. Parameters used in Fig. 5-10 are defined as follows:

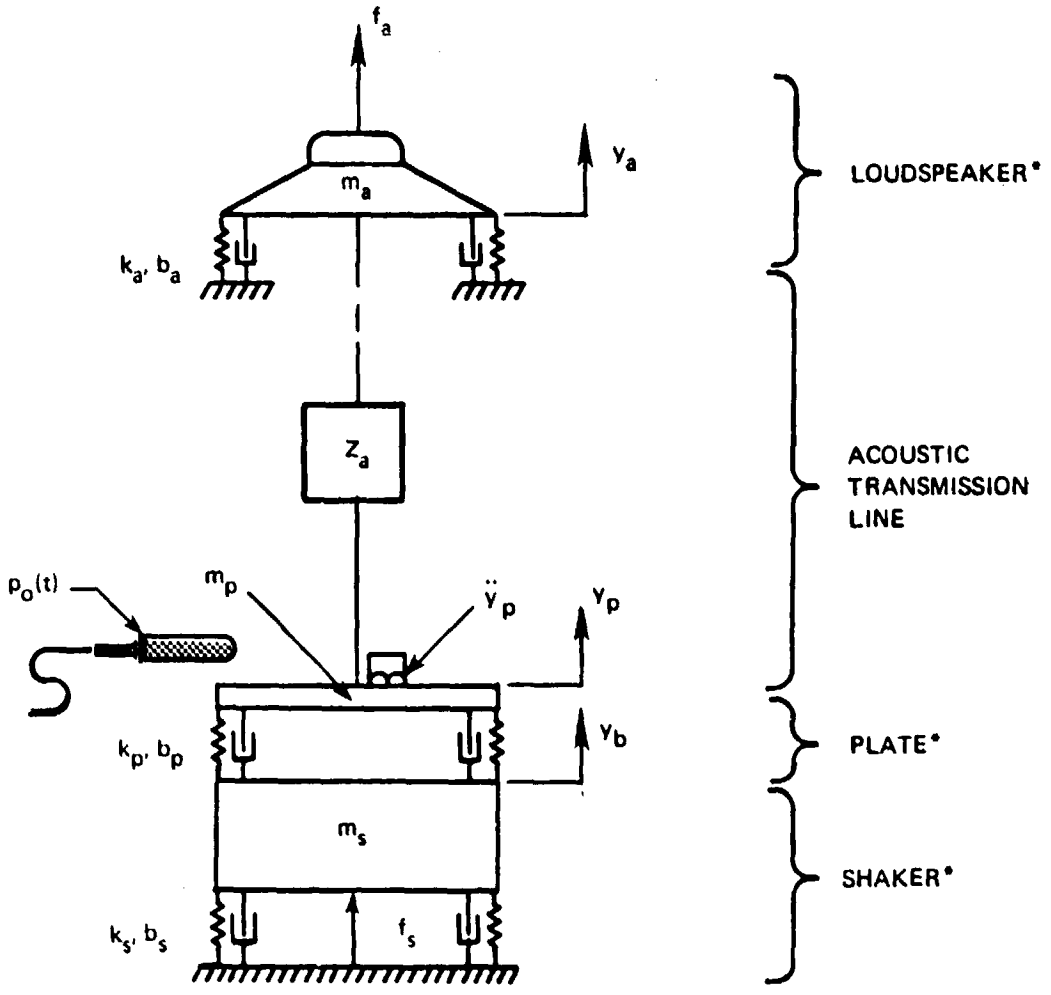

*FIRST MODE REPRESENTATION ONLY

Fig. 5-10 Model for Input Loading Analysis

f_a	magnetic force applied to speaker cone (zero input impedance)
m_a	mass of rigid speaker cone and exciter coil
k_a, b_a	stiffness, damping coefficients for cone suspension
Z_a	impedance of acoustic transmission line
m_p	plate mass associated with first plate mode
k_p, b_p	stiffness, damping coefficients associated with first plate mode
f_s	magnetic force applied to shaker armature (zero input impedance)
m_s	rigid body mass of shaker armature and plate fixture
k_s, b_s	stiffness, damping coefficients of shaker armature suspension

The analysis of the input loading phenomenon is most easily presented as two special cases: base excitation of the plate, ignoring the acoustic elements, and the acoustic excitation of the plate with the shaker input set to zero (blocked). These cases are considered below in sections 5.4.2.3 and 5.4.3.2.

5.4.2.3 Base Input Loading Analysis

An example of high resolution excitation and response spectra for a base input run was given in Section 5.4.2.1, as well as a broad description of the main features of the input loading effect. We proceed now to study the base input case in more detail.

Consider the case of base input only. The acoustic elements are assumed to be absent. The model of Fig. 5-10 simplifies to a two degree of freedom representation of the plate and shaker system. The plate system, by itself, has a natural frequency ω_p and damping

ratio ζ_p. The shaker system, by itself, has a natural frequency ω_s and damping ratio ζ_s. If the resonant frequencies of the shaker and of the plate are widely separated ($\omega_p >> \omega_s$), the fourth degree characteristic function which determines the coupled resonant frequencies of the combined system can be factored into two quadratic terms as follows:

$$\text{characteristic function} \approx (-\omega^2 + j2\zeta_\ell\omega_\ell + \omega_\ell^2)(-\omega^2 + j2\zeta_h\omega_h + \omega_h)^2 \qquad (5\text{-}6)$$

that is, the characteristic frequencies of the combined systems can be described by a lower resonant frequency $\omega_\ell < \omega_s$, and a higher resonant frequency $\omega_h > \omega_p$. The damping ratios of the separate systems, the shaker damping ratio ζ_s and the plate damping ratio ζ_p, are also affected when the shaker and plate are coupled. A first approximation to the relation between the separate and the coupled systems are:

$$\omega_\ell^2 \approx \omega_s^2 \left(1 - \frac{m_p}{m_s} - 4\zeta_s\zeta_p \frac{\omega_s}{\omega_p}\right) \qquad (5\text{-}7)$$

$$\zeta_\ell \approx \zeta_s \left[1 - \left(\frac{\omega_s}{\omega_p}\right)^2 \frac{b_p}{b_s}\right] \qquad (5\text{-}8)$$

$$\omega_h^2 \approx \omega_p^2 \left(1 + \frac{m_p}{m_s} - 4\zeta_s\zeta_p \frac{\omega_s}{\omega_p}\right) \qquad (5\text{-}9)$$

$$\zeta_h \approx \zeta_p \left[1 - \left(\frac{\omega_s}{\omega_p}\right)^2 \frac{b_p}{b_s}\right] \qquad (5\text{-}10)$$

The transfer functions for the base input and plate response accelerations can then be written as:

$$\ddot{y}_s = \frac{-\omega^2 f_s/m_s \ (-\omega^2 + j2\zeta_p\omega_p\omega + \omega_p^2)}{(-\omega^2+j2\zeta_\ell\omega_\ell\omega+\omega_\ell^2)(-\omega^2+j2\zeta_h\omega_h\omega+\omega_h^2)} \tag{5-11}$$

$$\ddot{y}_p = \frac{-\omega^2 f_s/m_s \ (j2\zeta_p\omega_p\omega+\omega_p^2)}{(-\omega^2+j2\zeta_\ell\omega_\ell\omega+\omega_\ell^2)(-\omega^2+j2\zeta_h\omega_h\omega+\omega_h^2)} \tag{5-12}$$

If now we evaluate these transfer functions near the plate resonant frequency $\omega_p \approx \omega_h >> \omega_\ell$, the following block diagram is obtained:

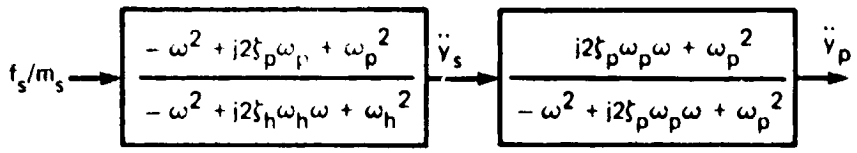

Figure 5-11 Base Excitation Block Diagram

Several aspects of this diagram are of particular importance. First, the transfer function on the left consists of a conjugate pair of zeros and a conjugate pair of poles. On the complex plane, these roots are very close to each other and also very close to the imaginary axis, since ω_h and ω_p differ only by very small quantities and the damping ratios ζ_h and ζ_p are <<1. The corresponding frequency response function has precisely the same antiresonant and resonant shape as base input curve (a) shown in Fig. 5-9. A second important aspect of the diagram is that the right hand transfer function precisely corresponds to the transfer function $H(\omega)$ shown as curves (d) and (e) on Fig. 5-9. The final and perhaps most important aspect of the diagram is the fact that if these two

transfer functions are cascaded to form a single transfer function between the shaker input force and the plate response acceleration, there will be a pole-zero cancellation associated with the plate frequency ω_p as shown in Fig. 5-12. This leads to the simple, and perhaps surprising result: since $\omega_p \approx \omega_h$, the transfer function shown in Fig. 5-12 is nearly that of a simple oscillator excited by a constant input acceleration f_s/m_s.

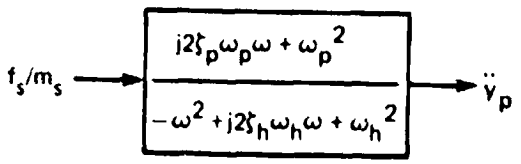

Figure 5-12 Shaker Force to Plate Acceleration Transfer Function

This particular input acceleration level is the value that would occur if the plate were to cause no loading effect at all. In essence, then, the net effect of the input loading effect on the plate resonance is to shift it slightly upwards in frequency from ω_p to ω_h. The magnitude of the plate resonance is virtually unchanged from the value it would have in response to an unloaded input f_s/m_s which is constant with frequency. So the effect of the input loading phenomenon on the plate response is rather minimal. However, the effect of the input loading phenomenon on the input to the plate remains problematic. As we have seen, the input loading effect suppresses the input sufficiently to allow the signal to be

contaminated by noise. It also complicates the problem of input identification because it is necessary to accurately resolve all the details of an input which varies very rapidly with frequency, and to match the peak and notch frequencies of the input curve very accurately with the plate response peak frequency.

5.4.2.4 Response and Input Identification Estimates for Base Excitation

The use of more accurate mode damping ratios and frequencies led to modest improvements in response estimates and substantial improvement in input identification estimates. The results of plate response experiments with base excitation are shown in Tables 5-5 and 5-6.

Table 5-5 High Resolution Base Input Test: Response PSD at Resonance

Mode No.	Response PSD at Resonance		Error
	Experimental	Program RAND	
1	3.6 g^2/Hz	5.13 g^2/Hz	+1.5 dB
2	9.18	7.14	-1.1
3	4.69	3.43	-1.4
4	4.19	3.02	-1.4

Table 5-6 High Resolution Base Input Test: Modal Response Power

Mode No.	Response Power		Error
	Experimental	Program RAND	
1	21.1 g^2	26.3 g^2	+ .96 dB
2	46.9	38.7	- .83
3	39.9	29.1	-1.4
4	39.3	21.5	-2.6
Overall	155.4	127.9	- .85

Table 5-5 shows the peak response PSD obtained by experiment and by RAND. These results represent an improvement over the results attainable by low resolution experiments (low resolution measurements of the sharply peaked power response spectra were typically in error by 12 to 16 dB). On the other hand, discrepancies between the theoretical and experimental modal power estimates (Table 5-6) are approximately the same as for the low resolution estimates (Table 5-3). As mentioned before, this is because the FFT algorithm computes the correct power of a signal independent of the degree of frequency resolution.

Substantial improvement in input identification accuracy is obtained by using high resolution FFT measurements. This improvement in accuracy is particularly evident at the plate resonant frequencies where large errors had previously existed due to inadequate resolution of input loading effects. In Figure 5-13, the RAND estimation of the base input in the region near each of the four plate resonances is compared with the measured input data. The plot is semi logarithmic. By comparing both the measured and identified base input power spectra to an arbitrary reference value, the ordinate can be scaled in dB as shown. The difference between the two curves can then be interpreted directly as an error expressed in dB. The rather coarse sampling of these two durves reflects the fact that the data link between the FFT analyzer and Program RAND was not automated and input/output data taking was done by hand. The accuracy of the input identification procedure, however, is satisfactory. An automated data link would improve the

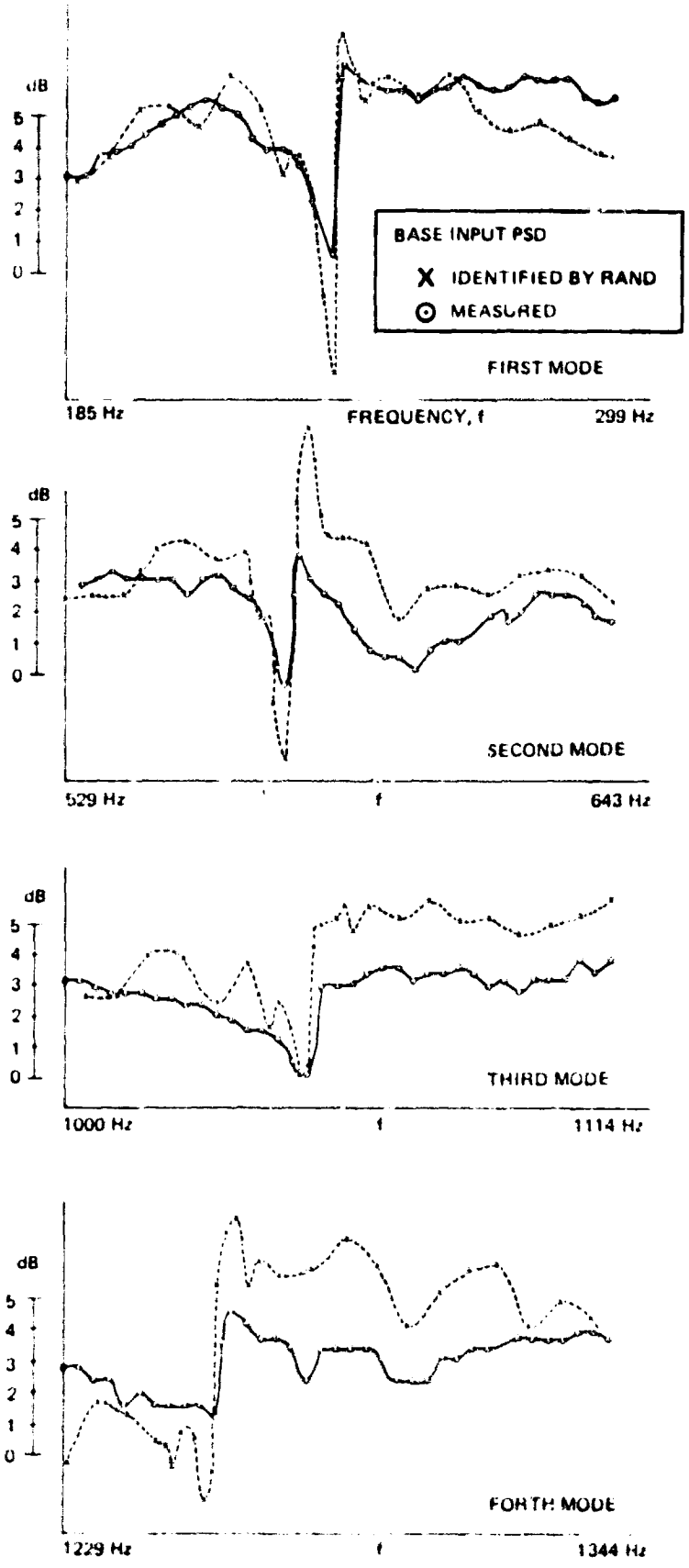

Fig. 5-13 High Resolution Identification of Base Input to Plate (Four Modes)

accuracy and resolution considerably. The measured overall power for the frequency band 0<f<2000 Hz was .60 g^2. The corresponding input identified by Program RAND was .524 g^2, which represents an overall error of -.59 dB.

5.4.3 Input Loading Effects: Acoustic Excitation Experiments

5.4.3.1 First Mode Input and Response Characteristics

An example of low resolution excitation and response data for an acoustic excitation test has already been given in Fig. 5-6. Two examples of high resolution data which show the effect of acoustic input loading on the first plate resonance are given in Figures 5-14 and 5-15. Broadly speaking, the acoustic loading effect is similar in pattern to the base input loading effect, although a closer study will reveal differences in detail. The actual shape of the loaded acoustic input, for instance, is different from the shape of the loaded base input curve. This is because the dynamics of the acoustic excitation differs from the base input dynamics. Dynamic models for the acoustic excitation of the plate are discussed in the next section and in the Appendix. An interesting contrast also exists between Figures 5-14 and 5-15. The first figure, which refers to the test condition of a blocked fixture (refer to Figure 5-10; y_b=0), exhibits a relatively mild acoustic loading effect. The second figure, which refers to the test condition of an unblocked fixture, exhibits a relatively strong acoustic loading effect. (The relative strength of the loading effect is measured by the depth of the antiresonant region of the pressure curve and by the corresponding amount of input noise

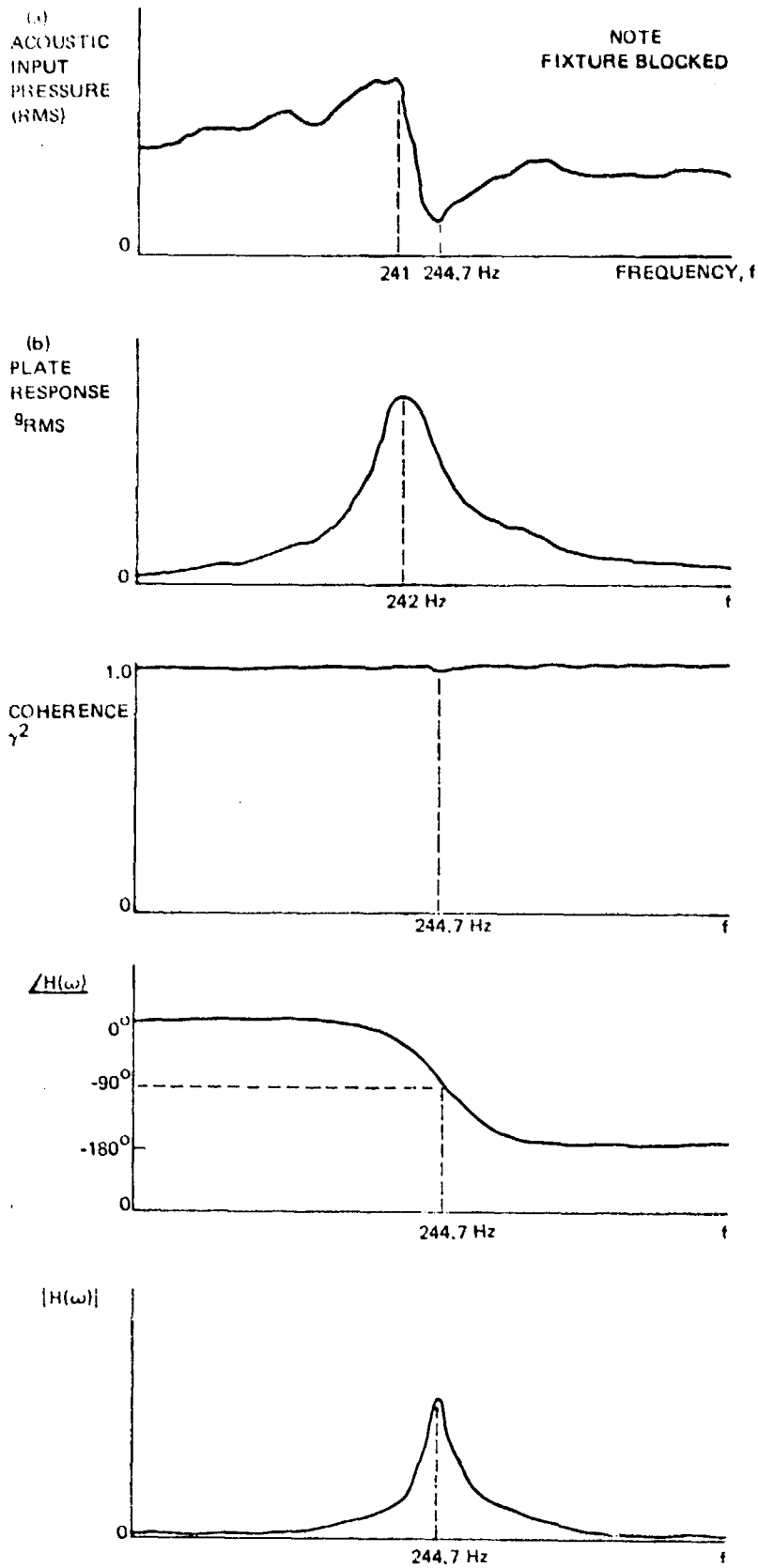

Fig. 5-14 High Resolution Spectra: Plate Response to Acoustic Input (First Mode, Fixture Blocked)

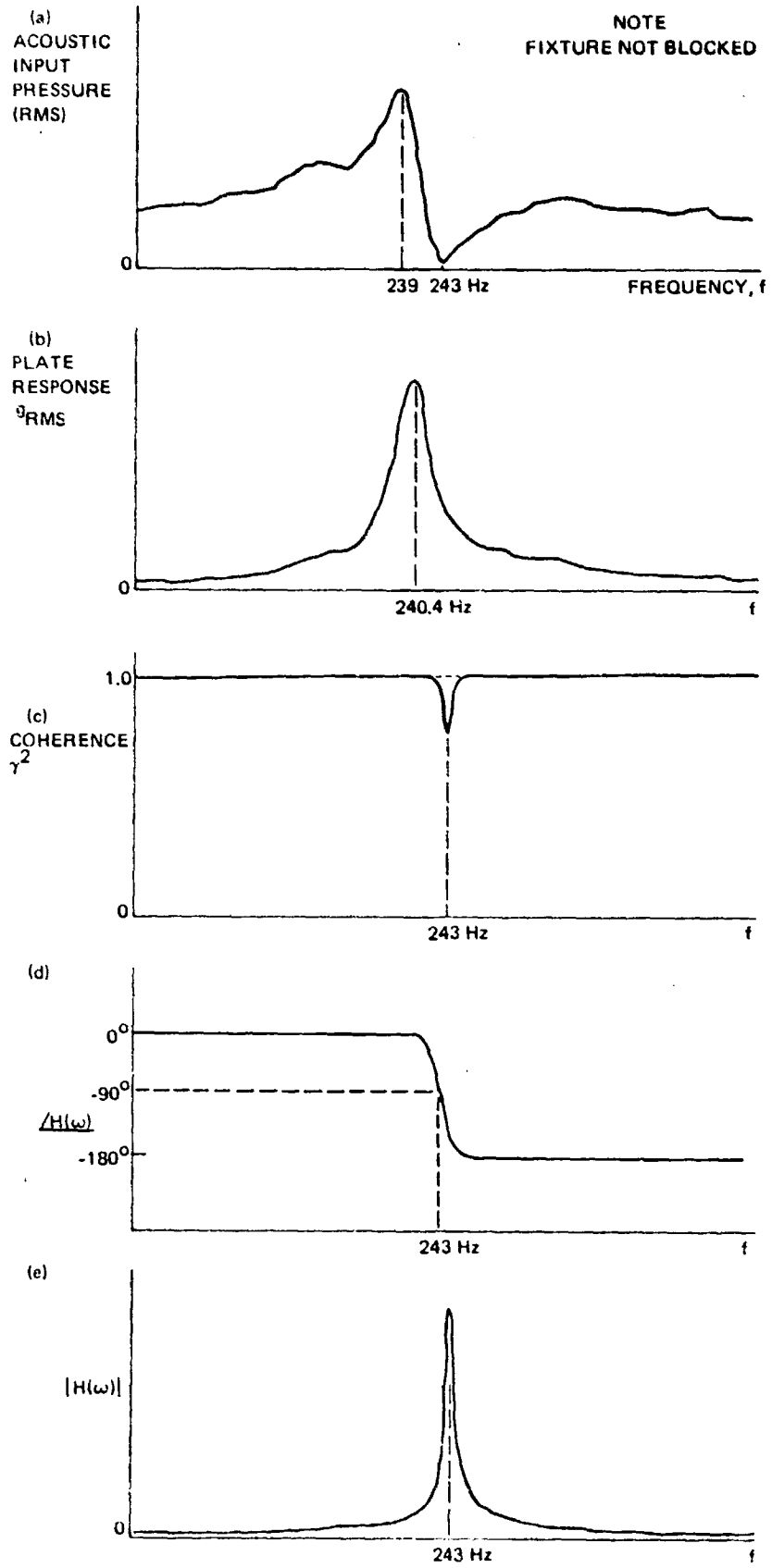

Fig. 5-15 High Resolution Spectra: Plate Response to Acoustic Input (First Mode, Fixture Not Blocked)

contamination, as evidenced by a decrease in coherence). The explanation for this difference is that the method of fixture restraint used in the blocked fixture test caused the damping level to be larger than that for the unblocked fixture test. This emphasizes the fact that the input loading phenomenon becomes more evident as the structural damping level decreases.

5.4.3.2 Acoustic Input Loading Analysis

Although the basic physical explanation for the acoustic input loading and the base input loading cases is similar, the acoustic and mechanical models required for the acoustic loading analysis is too complex to include in this section. These models are presented in some detail in Appendix A. Two acoustic excitation cases are of interest: excitation from a distant sound source which is not loaded by the plate generated sound waves, and excitation from a nearby sound source which is affected by the presence of the plate. The later case represents the experimental set up used in this study.

The results of the distant sound source analysis are presented in block diagram form, Fig. 5-16 (a). An incident pressure wave p_i emanates from the distant sound source. It is partially reflected by the moving plate. The resulting total pressure at the plate surface, p_o, is the sum of the incident and reflected wave pressures.

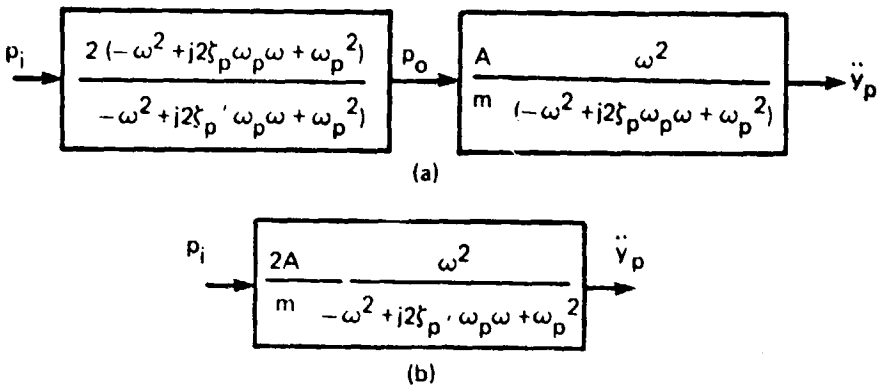

Figure 5-16 Acoustic Input Loading: Distant Source

The transfer function on the left again consists of a conjugate pole-zero pair. Although the undamped resonant frequency of the pole and the zero pairs are the same, the pole pair is more heavily damped. Specifically, the pole damping ratio

$$\zeta'_p = \frac{b_p + \rho cA}{2\sqrt{k_p m_p}} \tag{5-13}$$

includes both the material damping coefficient b_p of the plate and the acoustic radiation damping effect ρcA. The zero pair damping, on the other hand, includes only the plate material damping coefficient b_p. The frequency response characteristic of the left hand transfer function is a gain of 2 (perfect reflection) at all frequencies except at resonance, when it drops sharply down to the value $2b_p/(b_p+\rho cA)$. Thus an input loading effect exists

even though the distant acoustic source is not affected by the reflected wave from the plate. Such a frequency response characteristic does not cause a shift in frequency of the plate acceleration response peak. The transfer function on the right is again simply the transfer function for the plate under acoustic excitation. When cascaded, as in Fig. 5-16 (b), the plate acceleration response exhibits a single resonance, with the same amplitude it would have if excited by the incident pressure p_i without loading effect.

Next we consider the case of a nearby sound source (See Appendix for details). In Fig. 5-17 (a), a magnetic force f_a acts upon the loudspeaker cone, causing a pressure p_o to act upon the

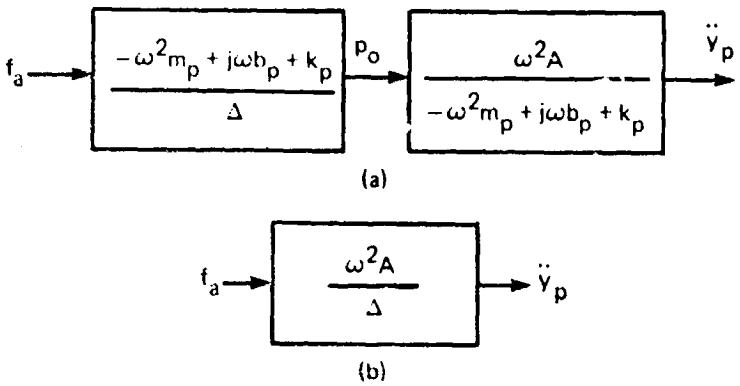

Figure 5-17 Acoustic Input Loading: Near Source

plate. The characteristic function Δ of the left hand transfer function is a complicated relation between the parameters which characterize the loudspeaker, the plate, and the connecting acoustic transmission line:

$$\Delta = \left[-(\rho cA\omega)^2 + (-\omega^2 m_a + j\omega b_a + k_a)(-\omega^2 m_p + j\omega b_p + k_p)\right] \sin \omega L/c$$
$$+ \rho cA\omega \left[-\omega^2(m_a+m_p) + j\omega(b_a+b_p) + (k_a+k_p)\right] \cos \omega L/c \qquad (5\text{-}14)$$

The resonant frequencies defined by the characteristic equation have not been evaluated explicitly, since a detailed evaluation of the many parameters would be required which is beyond the scope of this study. Note, however, that again the left hand transfer function which defines the pressure input to the plate consists of a conjugate pole-zero pair, and that again a pole-zero cancellation occurs when the two transfer functions are cascaded as shown in Fig. 5-17 (b). Our conclusion is again the same: although there is a complicated input loading interaction between the plate and the acoustically coupled loudspeaker system, the plate response is nearly the same as it would be if there were no input loading effect at all. The actual resonant frequency of the acoustically coupled plate differs slightly from the plate frequency which is excited by a distant pressure source. And again, the estimation of details of the acoustic input p_o remain problematic for reasons already stated above: the difficulties of estimating and measuring of high resolution narrow band spectra which vary rapidly with frequency.

5.4.3.3 Response Estimates for Acoustic Excitation

The acoustic input and the acceleration response of the plate were measured and compared with the plate response predictions of Program RAND. Table 5-7 shows the resonant peak PSD estimate comparisons for the first four plate resonances. Table 5-8 shows

Table 5-7 High Resolution Acoustic Input Test: Response PSD at Resonance

Mode No.	Response PSD at Resonance		Error
	Experimental	Program RAND	
1	.00748 g^2/Hz	.00616 g^2/Hz	-.087
2	.0283	.0156	-2.6
3	.0300	.0138	-3.4
4	.0240	.0432	+2.6

Table 5-8 High Resolution Acoustic Input Test: Modal Response Power

Mode No.	Response Power		Error
	Experimental	Program RAND	
1	.025 g^2	.024 g^2	-.18 dB
2	.084	.085	+.05
3	.234	.175	-1.26
4	.123	.503	+6.1

the integrated power comparison of each of the four resonances. These results are comparable to the plate response estimates obtained from base excitation tests. In both the base input and the acoustic input tests very close agreement between theory and experiment is possible. Yet it is also possible for substantial discrepancy to occur (up to 6 dB in one acoustic input case), even in spite of the fact that measurements were made with a high resolution analyzer. These large errors result mostly from imperfect characterizations of the sharply varying loaded inputs.

In an attempt to avoid the difficulties of measuring the sharply varying acoustic input spectra, an alternative method of characterizing the input was introduced: the taking of a simple average of the input PSD over a frequency bandwidth centered at the plate resonance. This approach requires less effort than the point-by-point characterization of the input, since the average is simply the ratio of the integrated power (obtained from the FFT analyzer by either a high resolution or a low resolution measurement) divided by the bandwidth. The approach also yields better results, as shown in Tables 5-9 and 5-10. A theoretical basis for the relative success of the bandwidth average approach has already been developed in the input loading studies in Sections 5.4.2.3 and 5.4.3.2. In both these analyses it was found that a sharply varying loaded input causes only a slight shift in the plate response resonance and does not significantly affect the response amplitude. It is reasonable that the loaded input can just as well be replaced by an equivalent input which is constant

Table 5-9 High Resolution Acoustic Input Test: Resonant Peak PSD Estimation Using Bandwidth Averaged Input

Mode No.	Response PSD at Resonance		Error
	Experimental	Program RAND	
1	.00748 g^2/Hz	.00743 g^2/Hz	-.03 dB
2	.0283	.0285	+.03
3	.0299	.0302	+.04
4	.0240	.0474	+2.95

Table 5-10 High Resolution Acoustic Input Test: Modal Power Estimation Using Bandwidth Averaged Input

Mode No.	Response Power		Error
	Experimental	Program RAND	
1	.025 g^2	.0257 g^2	+.12
2	.084	.113	+1.29
3	.234	.236	+.04
4	.123	.279	+3.5

with frequency. The easiest equivalent is a simple bandwidth averaged input. Further discussion of this simplified approach is presented below in Section 5.6.

5.5 Combined Base and Acoustic Excitation Experiments

The base excitation and the acoustic excitation were simultaneously applied to the plate at amplitudes which would each separately cause comparable response levels. Low resolution measurements were made of the pressure input PSD, the base acceleration PSD, the coincident and quadrature components of the cross PSD for the pressure and base inputs, and the integrated response power of the plate. These spectra are shown in Figures 5-18 through 5-20. No corresponding response estimates have been made using Program RAND.

Two aspects of these spectra are of interest. First, each of these inputs, applied separately, would cause comparable responses of the second, third and fourth modes. When these inputs are combined, however, the plate response shows a relatively enhanced second mode and a relatively attenuated third mode. This effect is caused by the phase relationship between the two inputs. Analysis of the response of a simple harmonic oscillator to statistically coupled inputs (Section 4.3.1) showed that the two inputs can either work together or work against each other, depending mostly on the sign and magnitude of the coincident component of the input cross power spectral density. A large negative coincident component will cause reinforcement of the inputs, whereas a large positive coincident component will tend to cause input cancellation. On this basis, the first mode should be suppressed, the second mode enhanced, the third mode unaffected, and the

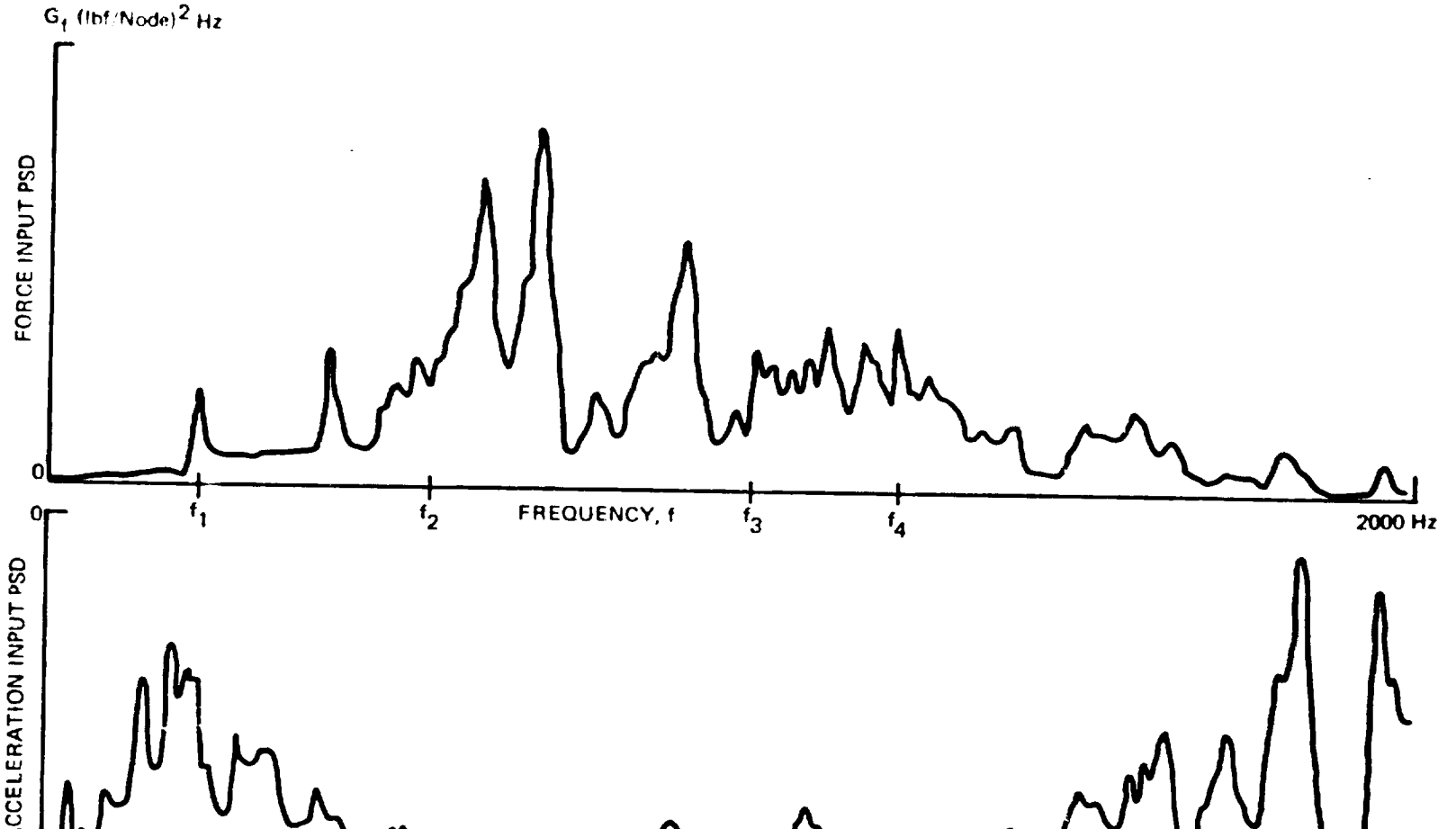

Fig. 5-18 Force and Acoustic Input Spectra for Combined Excitation of Plate

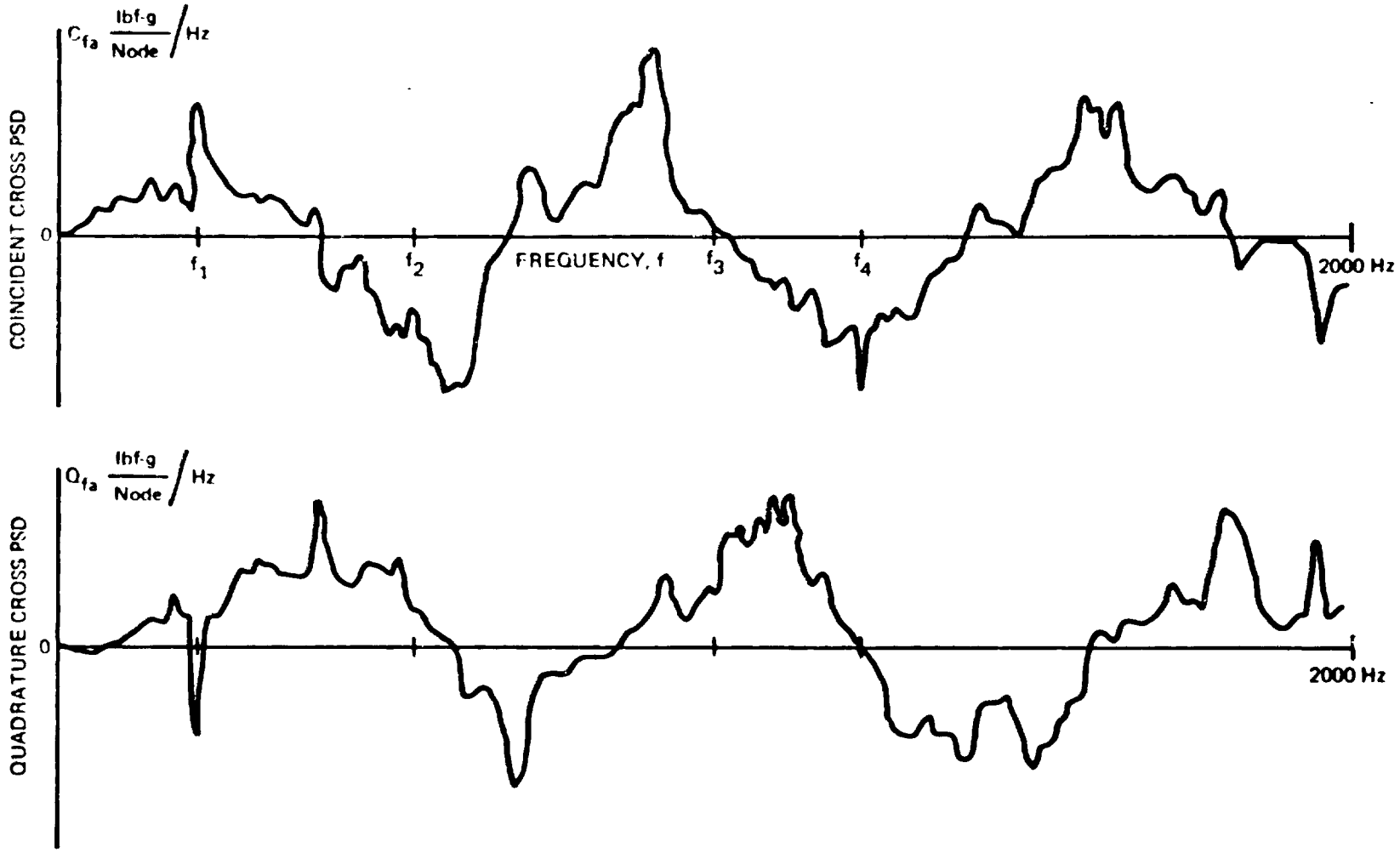

Fig. 5-19 Cross Spectra for Combined Force and Acoustic Inputs

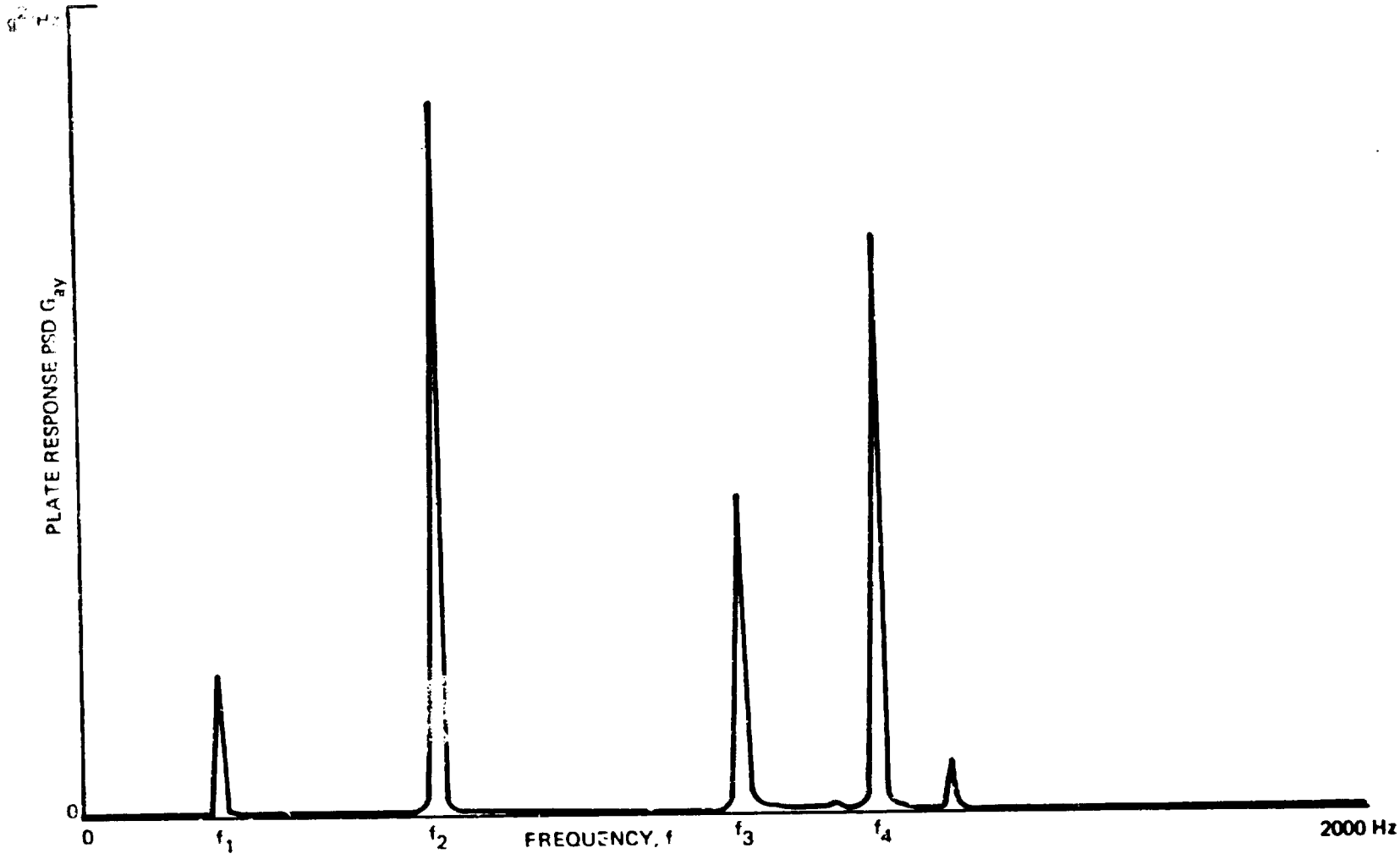

Fig. 5-20 Plate Response PSD for Combined Base and Acoustic Inputs

fourth mode strongly enhanced, each relative to the superposition of the response to the acoustic and base inputs applied separately. Roughly speaking, these effects appear consistent with the experimentally measured responses shown in Figure 5-20.

A second feature of the combined excitation spectra is the obvious presence of input loading effects at the resonant frequencies of the plate. This is particularly noticeable on the coincident and quadrature components of the input cross power (Figure 5-19) even though the low resolution FFT analysis would generally tend to obscure such effects.

It has already been established that it is difficult to obtain good response estimates when they are based on measured input spectra which experience input loading effects. The case will be no different as far as the input loaded cross power spectra are concerned. Although a bandwidth averaging technique offers some improvement for the case of individual input spectra, it remains to be demonstrated whether or not a similar procedure will be successful when cross input spectra are concerned.

5.6 Simplified Treatment of Input Loading Effects

We have already seen the effectiveness of using a simple bandwidth averaging technique when dealing with input loaded spectra. This technique simplifies the measurement procedure and leads to a better structural response estimate. Some questions remain, however. Analysis of the input loading phenomenon suggests that a constant, equivalent input spectrum can replace the sharply varying input loaded spectrum. The analysis does

C-2

not suggest, however, that the bandwidth average is the correct estimate of the constant, equivalent input. As damping decreases, for instance, the bandwidth average increases, whereas the theoretical value of the constant, equivalent input remains unchanged. There is also the practical question of determining a suitable bandwidth for the average. A larger bandwidth lessens whatever error may apply because the technique itself is not theoretically correct. On the other hand, a large bandwidth will tend to obscure input spectrum variations which have nothing to do with the input loading phenomenon. The answers to these questions will require further study. In the mean time, the bandwidth averaging technique offers a distinct improvement over precise point-by-point measurement of the input loaded spectrum.

What procedure should be followed when input identification estimates are to be made? Not only is such an identification of an input loaded spectrum difficult, but it would seem that it is also undesirable. It is of much more practical interest to identify the constant, equivalent input spectrum which will yield the same measured resonant response. In this case a theoretical guideline is available. For an isolated resonant mode excited by a white noise the acceleration response power is given by

$$\text{mode response power} = \frac{\pi \Gamma^2}{2} G_o f_n Q \qquad (5\text{-}15)$$

where Γ is the modal participation factor. In the input identification situation, the white noise input G_o, equivalent to the input loaded spectrum near the resonant mode, is to be estimated.

Rearrange eqn (5-15):

$$G_o = \frac{\text{Mode response power}}{\frac{\pi}{2} \Gamma^2 \ f_n \ Q} \qquad (5\text{-}16)$$

On the right hand side of eqn (5-16), the mode response power is measured, f_n and Q are known, and Γ is computed by Program RAND. So a theoretically correct constant equivalent input spectrum can be identified in simple fashion near the resonant mode. At non-resonant regions the problem of input loaded spectra does not exist and input identification can proceed in standard fashion using the input identification mode of Program RAND.

5.7 Conclusion to Part II

Implementation of the RAND procedure in an experimental situation brings in a wnole new set of problems: measurement accuracy, resolution, input loading effects, noise contamination of signals, and statistical averaging. Data show that given sufficient care and effort it is possible to obtain useful and meaningful response and input identification estimates.

The phenomenon of input loading proved to be significant experimentally and of definite interest theoretically. The simple analytical treatment of this phenomenon reflects the simple structures which comprised the laboratory set up. Work remains to be done to study the extent to which the present input loading models apply to complex field situations, for it is easy to speculate that input loading can have considerable practical significance. Imagine that a structural component undergoes vibration testing and then it is placed in a spacecraft for developmental flight testing or undergoes further vibration testing at a high structural integration level. In either case,

instrumentation is provided to characterize the base input level to the component. The results of this study have shown that a sharp peak can occur in the input spectrum due to an input loading effect, and that this peak, being slightly but critically detuned to the measured resonant frequency of the component, will have only a second order effect on the component resonant response. Now consider that the sharp input peak is discovered by an environmental specification writer, who routinely draws an envelope over it. An erroneous coincidence between the input peak and the component resonance is thereby guaranteed, and the resulting specification is substantially overestimated.

Finally, two considerations are added to give prospective to the experimental study described in Part II. First, we note that all of the experimental work was done without the benefit of a modern modal analysis system and without automatic data acquisition equipment. The former tool would have greatly improved the accuracy of the dynamical modelling of the structure. The latter tool, utilized to interface the FFT analyzer output directly to the computer, would have greatly increased the speed and ease of I/O operations with Program RAND, thereby making possible the use of the full resolution capabilities of the FFT analyzer. The second consideration is simply the recognition that it is important to distinguish between experimental work done in the laboratory, and experimental work done on much more complicated structures under field conditions. Obviously success in the laboratory does not guarantee success in the field.

Hopefully the techniques developed and knowledge gained in this study, coupled with improved hardware tools, will add to the success with which structural response and input identification estimates are made under real field conditions.

6.0 Summary

This study has focused on the problem of the response and input identification of a structure subjected to combined base and acoustic excitation. The study has included both theoretical and experimental approaches. Specific accomplishments are:

1. The development of a computer program RAND to make response and input identification estimates for a structure subjected to combined base and acoustic excitations.
2. The development of parametric design guidelines for plates subjected to random base or acoustic excitation.
3. Through a combination of analysis and experimentation, the evaluation of the applicability of the RAND procedure to a laboratory test situation, and the identification of the crucial considerations which affect the quality of structural input and response estimates.

Appendix A

A.1 Acoustic Input Loading Analysis

A.1.1 Case 1: Distant Sound Source

Refer to Figure 5-10: Model for Input Loading Analysis. Remove loudspeaker and acoustic transmission line, and set plate fixture displacement $y_b = 0$. The pressure $p_o(t)$ then acts on the effective area A for the first mode of the plate. The equation of motion is

$$m_p \ddot{y}_p + b_p \dot{y}_p + k_p y_p = -p_o A \qquad \text{(A-1)}$$

which leads to the transfer function

$$y_p/p_o = \frac{A}{m} \frac{\omega^2}{-\omega^2+j2\zeta_p\omega_p\omega+\omega_p^2} \qquad \text{(A-2)}$$

Next, relate pressure p_o with the incident pressure p_1 emanating from the distant sound source:

$$p_o = 2\, p_1 + \rho c \dot{y}_p \qquad \text{(A-3)}$$

that is, the total pressure p_o equals the incident and reflected wave pressures for the blocked plate plus the radiated pressure due to the plate velocity $\dot{y}_p$. Combine eqns (A-2) and (A-3) to obtain

$$p_o/2\, p_1 = \frac{-\omega^2+j2\zeta_p\omega_p\omega+\omega_p^2}{-\omega^2+j2\zeta_p'\omega_p\omega+\omega_p^2} \qquad \text{(A-4)}$$

where $\zeta_p' = (b_p + \rho cA)/m_p$

A.1.2 Case 2: Near Sound Source

Refer again to Figure 5-10. The system consists of the loudspeaker, acoustic transmission line, and plate. The plate fixture displacement $y_s = 0$. To facilitate the analysis we redraw the system and introduce a displacement function $\xi(x,t)$ for the acoustic transmission line as shown in Figure A-1.

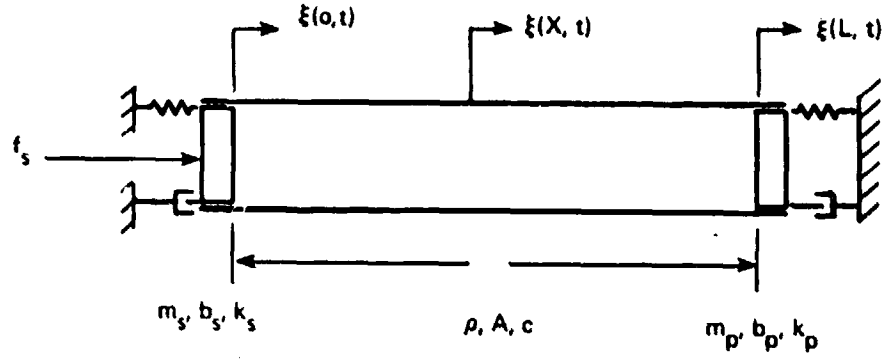

Figure A-1 Plate Excited by Near Sound Source

Assume that the dynamics of the air column can be described by the one dimensional wave equation

$$\frac{\partial^2 \xi}{\partial x^2} = \frac{1}{c^2} \frac{\partial^2 \xi}{\partial t^2} \tag{A-5}$$

subject to the boundary conditions

$$\xi(0,t) = \xi_1(t) = -y_a(t)$$

$$\xi(L,t) = \xi_2(t) = -y_p(t)$$

$$m_p \ddot{\xi}_2 + b_p \ddot{\xi}_2 + k_p \xi_2 + \rho c^2 A \frac{\partial \xi_2}{\partial x} = 0 \tag{A-6}$$

For a unit harmonic input the steady state response at x can be written as

$$\xi(x,t) = R_e \left[H(x,\omega)e^{j\omega t}\right] \tag{A-7}$$

The transfer function $H(x,\omega)$ can be evaluated by substituting eqn (A-7) into eqn (A-5) and then applying the boundary conditions (A-6):

$$H(x,\omega) = \cos \omega x/c + f(\omega) \sin \omega x/c \tag{A-8}$$

where $$f(\omega) = \frac{\rho Ac\omega \sin\omega L/c - (-\omega^2 m_p + j\omega b_p + k_p)\cos \omega L/c}{(-\omega^2 m_p + j\omega b_p + k_p)\sin \omega L/c + \rho Ac\omega \cos \omega L/c}$$

We are interested in the gage pressure

$$p_2 = -\rho_o c^2 \frac{\partial \xi}{\partial x}\Big|_{x=L} \tag{A-9}$$

which acts on the plate and the force f_a which acts on the loudspeaker. The loudspeaker force is obtained by requiring dynamic equilibrium for the forces which act on the loudspeaker mass:

$$f_a = m_a \ddot{\xi}_1 + b_a \ddot{\xi}_1 + k_a \xi_1 + p_1 A \tag{A-10}$$

where $p_1 = -\rho c^2 \frac{\partial \xi}{\partial x}\Big|_{x=0}$

For the case of harmonic motion

$$p_2 = \rho c\omega \left(-\sin \omega L/c + f(\omega) \cos \omega L/c\right) \tag{A-11}$$

$$f_a = \left(-\rho cA\omega\, f(\omega) - \omega^2 m_a + j\omega\, b_a + k_a\right) \tag{A-12}$$

The transfer function which relates the pressure which acts on the plate to the magnetic force which acts on the loudspeaker is then obtained by dividing (A-11) by (A-12):

$$p_2/f_a = -\rho c\omega \left(\frac{-\sin \omega L/c + f(\omega) \cos \omega L/c}{-\rho c\omega A\, f(\omega) - \omega^2 m_a + j\omega b_a + k_a} \right) \qquad \text{(A-13)}$$

Substitute the expression for $f(\omega)$ and simplify:

$$p_2/f_a = \frac{\rho c\omega \, (-\omega^2 m_p + j\omega b_p + k_p)}{\Delta} \qquad \text{(A-14)}$$

where

$$\Delta = [-(\rho cA\omega)^2 + (-\omega^2 m_a + j\omega b_a + k_a)(-\omega^2 m_p + j\omega b_p + k_p)] \sin \omega L/c$$

$$+ \rho cA\omega \, [-\omega^2 (m_a + m_p) + j\omega (b_a + b_p) + (k_a + k_p)] \cos \omega L/c$$

Appendix B

REFERENCES

1. Lyon, R.H., Statistical Energy Analysis of Dynamical Systems: Theory and Applications, MIT Press, 1975.

2. Lin, Y.K., Probabilistic Theory of Structural Dynamics, (McGraw-Hill), 1967.

3. Willig, S., Random Vibration of Point Driven Strings and Plates, Ph.D. Thesis, MIT, May 1971.

4. Crandall, S.H. (ed.), Random Vibration (Volume 2), MIT Press, 1963.